Article

Cell Systems

Inferring Metabolic Mechanisms of Interaction within a Defined Gut Microbiota

Graphical Abstract

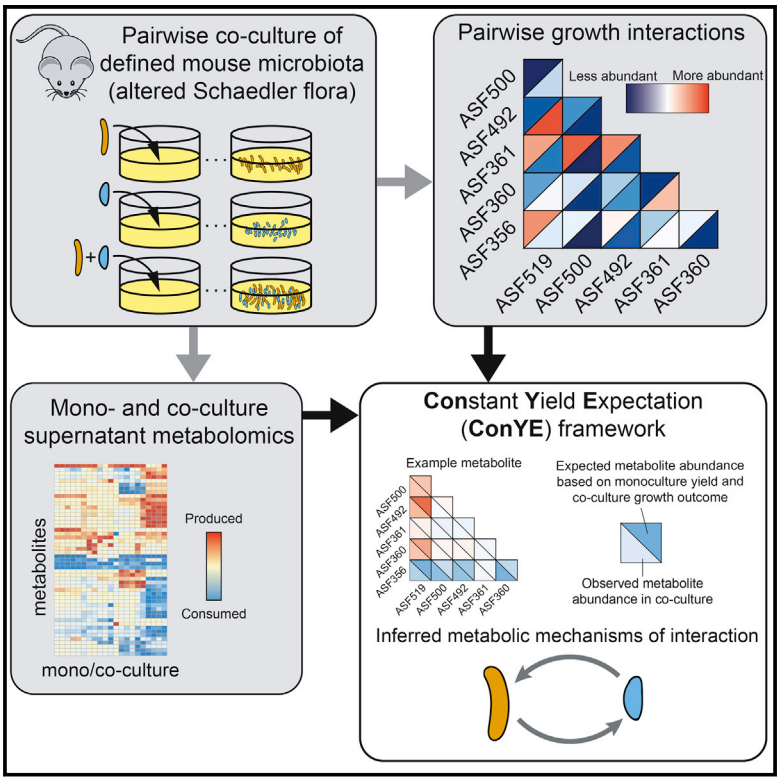

Highlights

- *In vitro* monoculture and co-culture of six members of a defined murine microbiota
- Growth and metabolome profiling to identify ecological and metabolic interactions
- Development and application of a constant yield expectation (ConYE) model
- Testing of inferred cross-feeding that contributed to commensal interaction

Authors

Gregory L. Medlock, Maureen A. Carey, Dennis G. McDuffie, ..., Jonathan R. Swann, Glynis L. Kolling, Jason A. Papin

Correspondence

papin@virginia.edu

In Brief

Ecological interactions determine the behavior of microbial communities, but pinpointing mechanisms governing these interactions is difficult. Here, we develop a framework for inferring interspecies metabolic interactions in co-culture based on monoculture behavior and co-culture growth outcomes. We profile the growth and metabolism of monocultures and co-cultures of bacteria from a defined mouse microbiota and apply our framework to these data. Based on these inferences, we investigate an amino acid cross-feeding interaction that may contribute to a commensal interaction.

Medlock et al., 2018, Cell Systems *7*, 1–13
October 24, 2018 © 2018 The Authors. Published by Elsevier Inc.
https://doi.org/10.1016/j.cels.2018.08.003

CellPress

Please cite this article in press as: Medlock et al., Inferring Metabolic Mechanisms of Interaction within a Defined Gut Microbiota, Cell Systems (2018), https://doi.org/10.1016/j.cels.2018.08.003

Cell Systems
Article

OPEN ACCESS
CellPress

Inferring Metabolic Mechanisms of Interaction within a Defined Gut Microbiota

Gregory L. Medlock,[1] Maureen A. Carey,[2] Dennis G. McDuffie,[1] Michael B. Mundy,[3] Natasa Giallourou,[4] Jonathan R. Swann,[4] Glynis L. Kolling,[1] and Jason A. Papin[1,5,6,7,*]
[1]Department of Biomedical Engineering, University of Virginia, Charlottesville, VA, USA
[2]Department of Microbiology, Immunology, and Cancer Biology, University of Virginia, Charlottesville, VA, USA
[3]Center for Individualized Medicine, Mayo Clinic, Rochester, MN, USA
[4]Department of Surgery and Cancer, Division of Integrative Systems Medicine and Digestive Diseases, Faculty of Medicine, Imperial College London, South Kensington, London, UK
[5]Department of Medicine, Division of Infectious Diseases & International Health, University of Virginia, Charlottesville, VA, USA
[6]Department of Biochemistry & Molecular Genetics, University of Virginia, Charlottesville, VA, USA
[7]Lead Contact
*Correspondence: papin@virginia.edu
https://doi.org/10.1016/j.cels.2018.08.003

SUMMARY

The diversity and number of species present within microbial communities create the potential for a multitude of interspecies metabolic interactions. Here, we develop, apply, and experimentally test a framework for inferring metabolic mechanisms associated with interspecies interactions. We perform pairwise growth and metabolome profiling of co-cultures of strains from a model mouse microbiota. We then apply our framework to dissect emergent metabolic behaviors that occur in co-culture. Based on one of the inferences from this framework, we identify and interrogate an amino acid cross-feeding interaction and validate that the proposed interaction leads to a growth benefit *in vitro*. Our results reveal the type and extent of emergent metabolic behavior in microbial communities composed of gut microbes. We focus on growth-modulating interactions, but the framework can be applied to interspecies interactions that modulate any phenotype of interest within microbial communities.

INTRODUCTION

The structure and function of microbial communities may influence human health through a variety of means (Turnbaugh et al., 2007). However, understanding the mechanisms governing this influence is complicated by the complexity of microbial communities. Interspecies interactions within microbial communities underlie benefits to human health, such as colonization resistance to pathogens (Britton and Young, 2014; Buffie and Pamer, 2013). These interspecies interactions are often metabolic, such as competition for metabolites essential for the growth of pathogens (Gillis et al., 2018; Lawley and Walker, 2013; Stecher and Hardt, 2008). Since metabolic interactions occur between distantly (Fischbach and Sonnenburg, 2011) and closely related (Rakoff-Nahoum et al., 2014) species, creating heuristics for identifying the presence or absence of interactions based on phylogeny is challenging. Knowledge of interactions among small subsets of community members has been shown to enable prediction of community assembly in larger communities, suggesting that constructing predictive models of population dynamics in complex microbial communities may be a tractable problem (Friedman et al., 2017). However, in this same study, while pairwise interactions were sufficient to predict community assembly in three-species pairs, information from three-species communities was necessary to predict assembly of larger communities. Further supporting the lack of generalizability of pairwise interactions to new conditions, theoretical ecological analyses suggest that universal interspecies interaction terms in pairwise ecological interaction models cannot recapitulate commonly identified chemical-mediated interspecies interactions (Momeni et al., 2017). Thus, generalizable methods for predicting assembly of large microbial communities likely depend on more mechanistic knowledge of interactions that can help account for context specificity, such as the consumption and production of metabolites that might be shared within a community (Goldford et al., 2018).

The spatial, temporal, and compositional complexity of microbial communities in mammals makes inferring mechanisms of interaction challenging. Using gnotobiotic animals can improve the tractability of this problem. However, knowledge of the behavior of individual microbes within the defined community is generally lacking unless classical model organisms are used in place of naturally occurring organisms. To increase the value of experiments performed using gnotobiotic animals, individual members of the microbiota can be characterized *in vitro*. The phenotyping performed via these experiments improves our understanding of these organisms, which may improve our ability to predict and interpret how they might behave *in vivo*.

The altered Schaedler flora (ASF) is a group of eight bacterial strains isolated from the mouse gastrointestinal tract used to standardize the microbiota of laboratory mice (Wymore Brand et al., 2015). ASF-colonized mice remain stably colonized across mouse generations and have normalized organ physiology relative to germ-free mice (Wymore Brand et al., 2015). Although

This is an open access article under the CC BY license (http://creativecommons.org/licenses/by/4.0/).

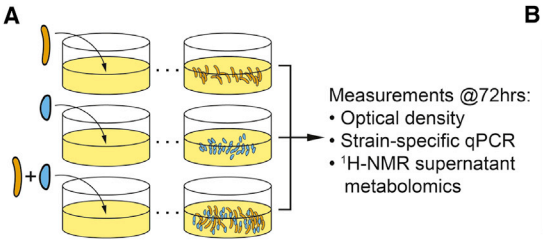

B

ASF strain	taxonomy
ASF356	*Clostridium sp.*
ASF360	*Lactobacillus intestinalis*
ASF361	*Lactobacillus murinus*
ASF492	*Eubacterium plexicaudatum*
ASF500	*Pseudoflavonifractor sp.*
ASF519	*Parabacteroides goldsteinii*

Figure 1. Summary of Co-culture Experiment Design, Measurements, and Total Growth Outcomes in Monocultures and Co-cultures

(A) Experimental procedures for each pair of strains and measurements taken.

(B) Taxonomic assignment for strains included in this study.

there are known differences between the immune repertoires of ASF-colonized mice and conventional mice, these differences can be exploited to test specific hypotheses (Geuking et al., 2011; Ivanov et al., 2009). ASF mice have been used widely in infectious disease research to study *Clostridium difficile* (Schwan et al., 2009), *Salmonella enterica* (Brugiroux et al., 2016), and *Cryptosporidium parvum* (Harp et al., 1992). Many specific pathogen-free mice are initially colonized with the ASF, which has led to the theory that the presence or absence of ASF strains contributes to vendor-specific differences in susceptibility to disease (Singer and Nash, 2000). Further use of gnotobiotic systems such as the ASF-colonized mice could greatly accelerate discovery in microbiome research, especially if the behavior of the ASF alone is well understood.

Previously, we performed pairwise spent media experiments using seven of the ASF strains, in which each strain was grown in the same medium as well as the spent medium of other strains (Biggs et al., 2017). We identified cases of putative cross-feeding and competition and the effect of those interactions on growth dynamics. However, each strain was spatially and temporally separated in that study. While spent media experiments remove some technical and statistical complications in inferring metabolic interactions, the interactions that are possible are different than those that might occur while strains are grown in co-culture.

Here, we further define the interactive potential of six of the ASF strains and develop an analytic method to infer putative mechanisms of metabolic interaction. We perform co-culture growth experiments with all pairs of these strains and profile their supernatant metabolomes in both monoculture and co-culture. We identify the influence of interspecies interactions on the growth of each strain and then apply our analytic framework for inferring putative metabolic mechanisms of interaction from supernatant metabolomic data. We experimentally interrogate an inferred cross-feeding interaction in which one ASF strain (*Parabacteroides goldsteineii* ASF519) produces amino acids that another (*Clostridium sp*. ASF356) consumes, confirming that the hypothesized mechanism occurs and leads to a growth benefit for the consuming strain. With this new insight, we provide a framework to identify putative metabolic mechanisms of microbe-microbe and host-microbe interactions that can be applied to any microbial community to investigate co-culture phenotypes including growth enhancement or changes in metabolite yield.

RESULTS

Ecological Interactions within the Altered Schaedler Flora

We collected *in vitro* data for growth of all monocultures and pairwise combinations of six ASF strains (Figure 1A, n = 6–9 per strain pairing). Taxonomic assignments for these strains are provided in Figure 1B, and we refer to them by their genus and strain number. We determined the impact of co-culture on each strain's growth by comparing monoculture abundance after 72 hr of growth to the abundance of each strain in co-culture at the same time (determined using probe-based qPCR; all strains are in stationary phase; see example growth curves in Figure S2; see STAR Methods).

The abundance of each strain in each pair was evaluated to determine whether a negative (−), positive (+), or neutral (0) effect on abundance occurred in the pairing, allowing classification of pairwise interaction with standard ecological terminology. All pairings except one, *Clostridium* ASF356 with *Parabacteroides* ASF519, had a negative impact on the abundance of at least one strain, with 0/− (amensalism), +/− (parasitism), −/− (competition), and +/0 (commensalism) being the only interactions detected (8, 4, 2, and 1 instances, respectively; data shown in Figure 2A, summarized in 2B and 2C). *Lactobacillus* ASF361 was present in three out of four parasitic co-cultures and experienced a growth benefit in all cases. In contrast, the growth of both *Eubacterium* ASF492 and *Pseudoflavonifractor* ASF500 was inhibited in every condition, including in co-culture with each other. In summary, the abundance of individual strains tended to be lower in co-culture than in monoculture. However, the growth benefit observed for some strains also suggests that differences in resource utilization across strains, or emergent behavior in co-culture such as cross-feeding and consumption of novel metabolites, occurred in some co-cultures.

Metabolic Repertoires within the Altered Schaedler Flora

To determine potential mechanisms governing the changes in growth observed in co-culture, we performed metabolomics on the spent supernatant from all samples in the growth experiments (using ^{1}H NMR [hydrogen-1 nuclear magnetic resonance] spectroscopy, see STAR Methods). We updated and refined the metabolite peak annotations from experiments previously performed using the same medium and strains (Biggs et al., 2017), resulting in 86 detected metabolites, 50 of which could be assigned an identity (36 of 85 metabolites were previously assigned an identity). We identified new metabolites involved in amino acid metabolism (serine, cysteine, asparagine, glutamate, 2-oxoisocaproate, and isocaproate), nucleic acid metabolism (cytidine, cytosine, and uridine monophosphate), and anaerobe-specific metabolism (isopropanol).

Based on the monoculture supernatant metabolomic profiles presented here (Figure 3A) and in our previous study of the ASF, the ASF strains have fermentation repertoires similar to closely related gut microbes (Biggs et al., 2017). *Lactobacillus*

Please cite this article in press as: Medlock et al., Inferring Metabolic Mechanisms of Interaction within a Defined Gut Microbiota, Cell Systems (2018), https://doi.org/10.1016/j.cels.2018.08.003

OPEN ACCESS
CellPress

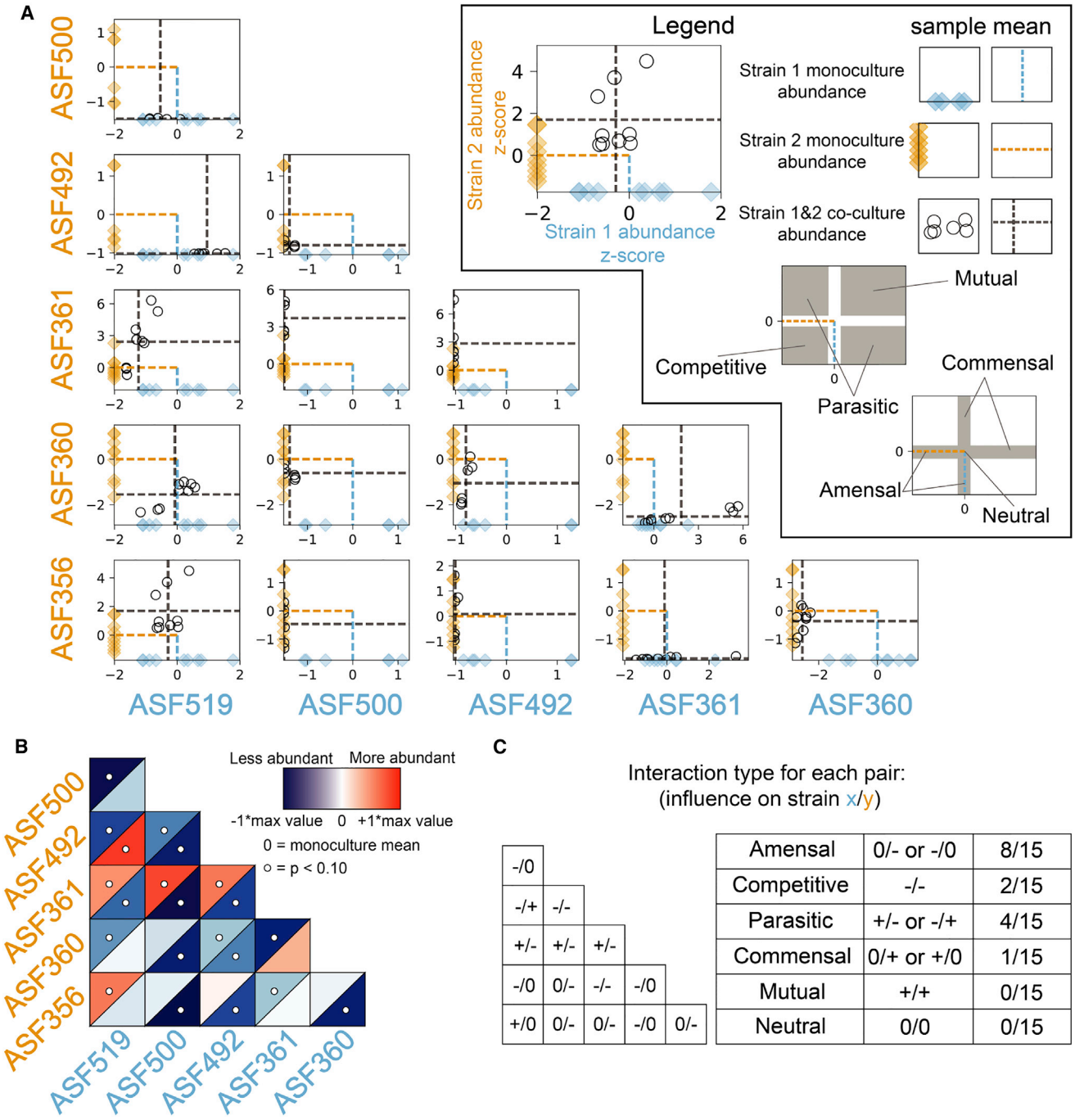

-/0				
-/+	-/-			
+/-	+/-	+/-		
-/0	0/-	-/-	-/0	
+/0	0/-	0/-	-/0	0/-

Amensal	0/- or -/0	8/15
Competitive	-/-	2/15
Parasitic	+/- or -/+	4/15
Commensal	0/+ or +/0	1/15
Mutual	+/+	0/15
Neutral	0/0	0/15

Figure 2. The Effects of Pairwise Co-culture on the Abundance of Each Strain

(A) Relative abundance of each strain in monoculture and co-culture determined via qPCR. Abundance is plotted on a linear scale, not log-transformed. X axis describes the abundance of strain at the bottom of the column; y axis describes the abundance of the strain at the left of each row. Diamonds indicate the abundance of each strain in monoculture, with the mean shown by a dashed line. The abundance of each strain in co-culture as indicated by the row and column labels is shown by a black circle, with mean abundances indicated by gray dashed lines. Abundance for each strain is *Z* score normalized using mean and standard deviation of monoculture abundance to center and scale the data, respectively. n = 9 for all samples except for those with *Pseudoflavonifractor* ASF500 or *Eubacterium* ASF492, for which n = 6.

(B) Heatmap of the mean abundance of each strain in co-culture relative to monoculture. Blue indicates less abundant while red indicates more abundant than monoculture. The upper left and lower right triangles in each square describe the abundance of the strain labeled on the left of row and bottom of the column, respectively. White circles indicate differential abundance between monoculture and co-culture ($p < 0.10$, Mann-Whitney U test with false discovery rate correction using Benjamini-Hochberg procedure).

(C) Summary of interspecies interactions. Non-zero interactions in the triangular matrix indicate significant differential abundance as shown in Figure 2B.

Please cite this article in press as: Medlock et al., Inferring Metabolic Mechanisms of Interaction within a Defined Gut Microbiota, Cell Systems (2018), https://doi.org/10.1016/j.cels.2018.08.003

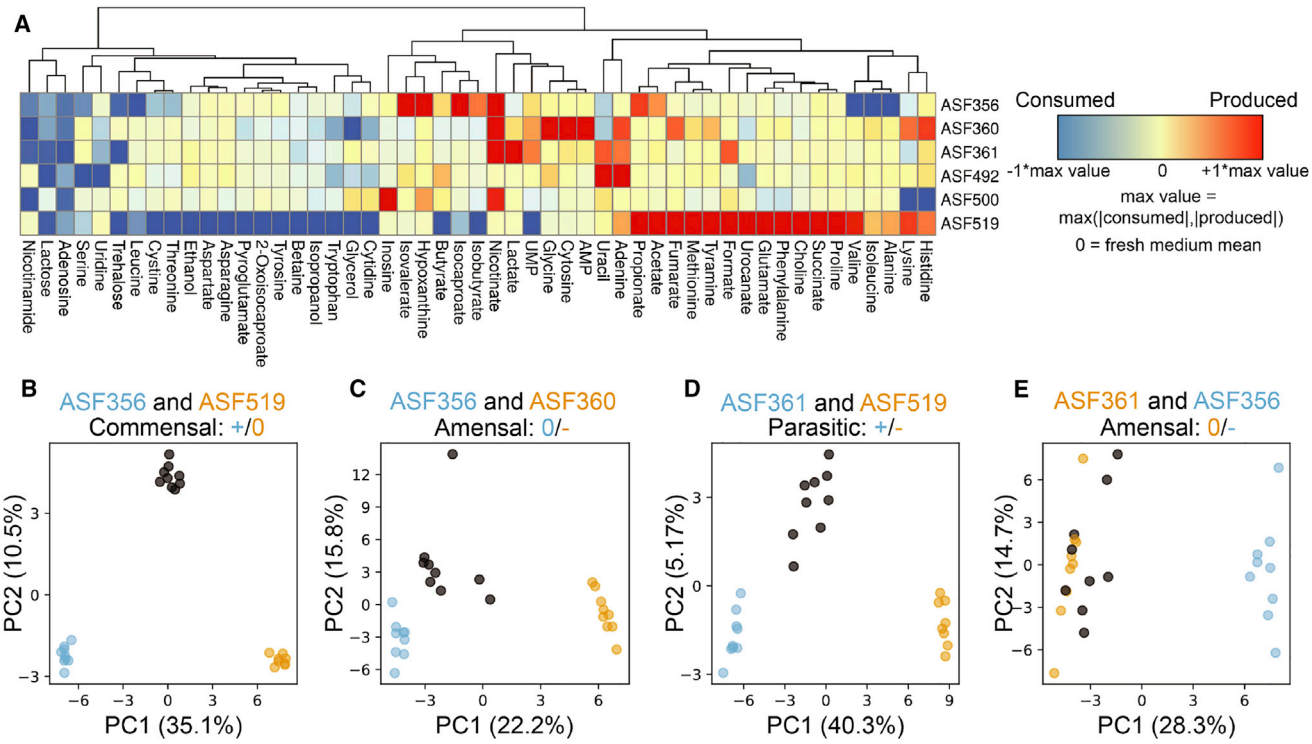

Figure 3. Metabolic Behavior of Each Strain in Monoculture and Emergent Behavior in Co-cultures

(A) Heatmap describing supernatant metabolomes for each monoculture. Red and blue indicate higher or lower concentrations than fresh medium, respectively. Values are centered at 0 using the mean in fresh media, then scaled between −1 and +1 by dividing by the maximum change in concentration for each metabolite in any sample in the study. Unnamed metabolites are not shown. Hierarchical clustering was performed using Euclidean distances and complete linkage.

(B–E) Principal-component analysis (PCA) of monocultures and co-culture, performed independently for each subplot. Sky blue and orange circles correspond to monoculture supernatant metabolomes from strain labeled with the same color. Co-culture samples for the two strains in each subplot title are indicated by gray circles. Percent variance captured by each principal component is labeled on each axis.

ASF360 and *Lactobacillus* ASF361 both produced lactate, while *Lactobacillus* ASF361 also produced acetate and formate. Other strains of *Lactobacillus intestinalis* and *Lactobacillus murinus* are generally identified as facultative heterofermentative lactic acid bacteria (Vos et al., 2011). Heterofermentative lactic acid bacteria ferment carbohydrates to lactate but may also produce additional acetate in some conditions. *Clostridium* ASF356 produced the common fermentation end products acetate, propionate, succinate, and butyrate. Butyrate production is common in *Clostridia* that inhabit mammalian gastrointestinal tracts and is often coupled with acetate production (Louis and Flint, 2009). Propionate is the primary end product of three common pathways identified in anaerobic organisms, of which the acrylate pathway and succinate pathway have been identified in *Clostridia spp.* (Reichardt et al., 2014). *Clostridium* ASF356 also produced isovalerate, isocaproate, and isobutyrate, which are common products of amino acid fermentation by some *Clostridia spp.* (Mead, 1971). Butyrate and ethanol were the only common fermentation end products produced by *Eubacterium* ASF492. *Eubacterium* ASF492 has been proposed as the type strain for *Eubacterium plexicaudatum* (Dewhirst et al., 1999), which was originally identified as producing butyrate and small amounts of acetate from glucose (Wilkins et al., 1974). *Pseudoflavonifractor* ASF500 produced only formate and consumed less lactose than any other ASF strain, suggesting that lactose is not a preferred carbon source for *Pseudoflavonifractor* ASF500 or that another growth-limiting nutrient is only present at low abundance in the medium. *Parabacteroides* ASF519 produced acetate, propionate, and succinate, consistent with previous reports on fermentation products of *P. goldsteinii* (Song et al., 2005), as well as formate. *Parabacteroides* ASF519 also produced many amino acids, including histidine, lysine, alanine, isoleucine, valine, proline, phenylalanine, glutamate, and methionine, suggesting *Parabacteroides* ASF519 contains a comprehensive amino acid biosynthesis repertoire.

Co-culture Can Lead to Emergent Metabolic Behavior

Co-culture substantially altered the metabolome of pairings relative to each of the monoculture metabolomes for the strains involved (see Figure S1 for results from all groups). To detect and quantify the emergent metabolic behavior resulting from co-culture, we performed principal-component analysis (PCA) (see STAR Methods) on the metabolic profile for pairs of strains. We performed PCA separately for each pair of strains, including samples from each monoculture and the co-culture. In cases where both strains grew in co-culture (i.e., no strong negative growth effect), the first principal component (PC1) separated monocultures by strain, and the second principal component (PC2) separated monoculture samples from co-culture samples. This behavior was particularly strong in the case of *Clostridium*

ASF356 and *Parabacteroides* ASF519 (Figure 3B). For *Clostridium* ASF356 and *Parabacteroides* ASF519, the loadings of PC2 suggest that co-culture increased production of propionate, glycine, and the amino acid fermentation products isovalerate, isocaproate, and isobutyrate and increased consumption of multiple amino acids and lactose.

For pairings with a strong negative effect on one strain, the co-culture metabolomes were less similar to the negatively affected strain than the other strain. For example, co-culture of *Clostridium* ASF356 with *Lactobacillus* ASF360 resulted in decreased growth of *Lactobacillus* ASF360, and the co-culture samples are located closer to *Clostridium* ASF356 monoculture samples in PCA (Figure 3C). Although there is still an "emergent" co-culture effect observed in PC2 for this pair, the effect is also aligned with within-group variation. The same trend is present for *Lactobacillus* ASF361, *Parabacteroides* ASF519, and their co-culture (Figure 3D). For strong negative growth outcomes (e.g., *Clostridium* ASF356 and *Lactobacillus* ASF361 co-culture), the effect is more pronounced, and there is less separation between monoculture and co-culture samples (Figure 3E).

Development of an Expectation-Based Model to Account for Changes in Strain Abundance

Based on the metabolic differences between monoculture and co-culture samples identified via PCA, co-culture conditions substantially altered metabolic behavior. However, the mechanism that leads to this emergent metabolic behavior is unclear, and attempting to infer the mechanism may be confounded by changes in the abundance of each strain in co-culture. We sought to infer metabolic interactions between strains in co-culture by accounting for changes in strain abundance. While the absolute amount of a metabolite produced or consumed may change in co-culture relative to monoculture, taking changes in strain abundance into account is necessary to determine whether the change in metabolite abundance is emergent behavior rather than additive.

We developed a constant yield expectation (ConYE) model to identify metabolites for which consumption or production behavior changed in co-culture (see STAR Methods). Within the ConYE model, we assume each strain produces or consumes a fixed quantity of each metabolite per unit biomass (i.e., constant yield), then test whether that assumption is true in co-culture by comparing the expected behavior to the observed co-culture data. We simulate expected metabolite quantities in co-culture by multiplying the monoculture-derived metabolite yield for each strain by the observed abundance of that strain in co-culture, then summing up the expected values for each strain and the initial quantity of the metabolite present in the fresh medium (Figure 4A). For each metabolite, we test the null hypothesis that the quantity of that metabolite in co-culture is equal to that predicted by the ConYE model. Rejecting the null hypothesis for a metabolite implies that co-culture caused at least one strain to alter the metabolism of that metabolite relative to its own biomass production.

We identified several patterns with the ConYE model results that were consistent across sets of many metabolites, for which representative examples are shown (Figure 4B). Metabolites consumed in monoculture were often consumed less than expected in co-culture, especially when one strain in the co-culture experienced a growth benefit (e.g., lactose). For some strains, this pattern may arise because alternative metabolites are now available in co-culture that can be consumed to produce biomass, decreasing the amount of lactose required to produce a unit of biomass. Similarly, another pattern involves fermentation end products, which were generally less abundant than expected. Lactate, which was produced by *Lactobacillus* ASF360 and *Lactobacillus* ASF361, was less abundant than expected in seven out of nine co-cultures containing either strain. Explanations for this pattern align with explanations for the first pattern; individual strains may utilize alternative metabolites to produce biomass, resulting in less production of primary fermentation products. An alternative explanation is that other strains in the co-culture are consuming the fermentation end product, as may be the case for lactate (*Clostridium* ASF356, *Eubacterium* ASF492, and *Parabacteroides* ASF519 consumed lactate in the fresh medium). Similar explanations may fit the behavior of other metabolites that are not end products of fermentation, such as valine. Valine was consumed by some strains and produced by others, but the null hypothesis for valine was only rejected for 3 out of 15 co-cultures. In cases where one strain produced a metabolite in monoculture (e.g., *Parabacteroides* ASF519 producing valine) and another strain consumed the metabolite in monoculture (e.g., *Clostridium* ASF356 consuming valine), failure to reject the null hypothesis even when one strain experienced a growth benefit (e.g., *Clostridium* ASF356 co-cultured with *Parabacteroides* ASF519) suggests that a metabolite may have been cross-fed.

As demonstrated by these examples, interpretation of ConYE can be informed by considering the direction of metabolite abundance change in monoculture. If either strain consumed a metabolite in monoculture (Figure 4C, left, all co-cultures shown), rejecting the null hypothesis implies the metabolite was consumed more or less than expected or that one of the strains produced the metabolite in co-culture (e.g., emergent production). Conversely, if either strain produced a metabolite in monoculture (Figure 4C, middle), rejecting the null hypothesis implies the metabolite was produced more or less than expected or that one of the strains consumed the metabolite in co-culture (which was not observed in monoculture for that strain). For both the production and consumption cases, cross-feeding was still possible but required emergent consumption or production by one strain.

When a metabolite was consumed by one strain in monoculture and produced by the other strain in monoculture (Figure 4C, right), there are four possible interpretations if the null hypothesis is rejected. If the metabolite was less abundant than expected, then at least one of two conclusions is true: (1) the consumer metabolized more of the metabolite than expected, or (2) the producer produced less. If the metabolite was more abundant than expected, the opposite is true (the producer produced more, or the consumer consumed less). If the null hypothesis is not rejected, the strains either maintained their production and consumption behavior from monoculture or both scaled their consumption and production up or down in equal amounts. These interpretations, as well as their corresponding importance or relative contribution to a positive growth interaction for the consuming strain, are summarized in Figure 5.

OPEN ACCESS
CellPress

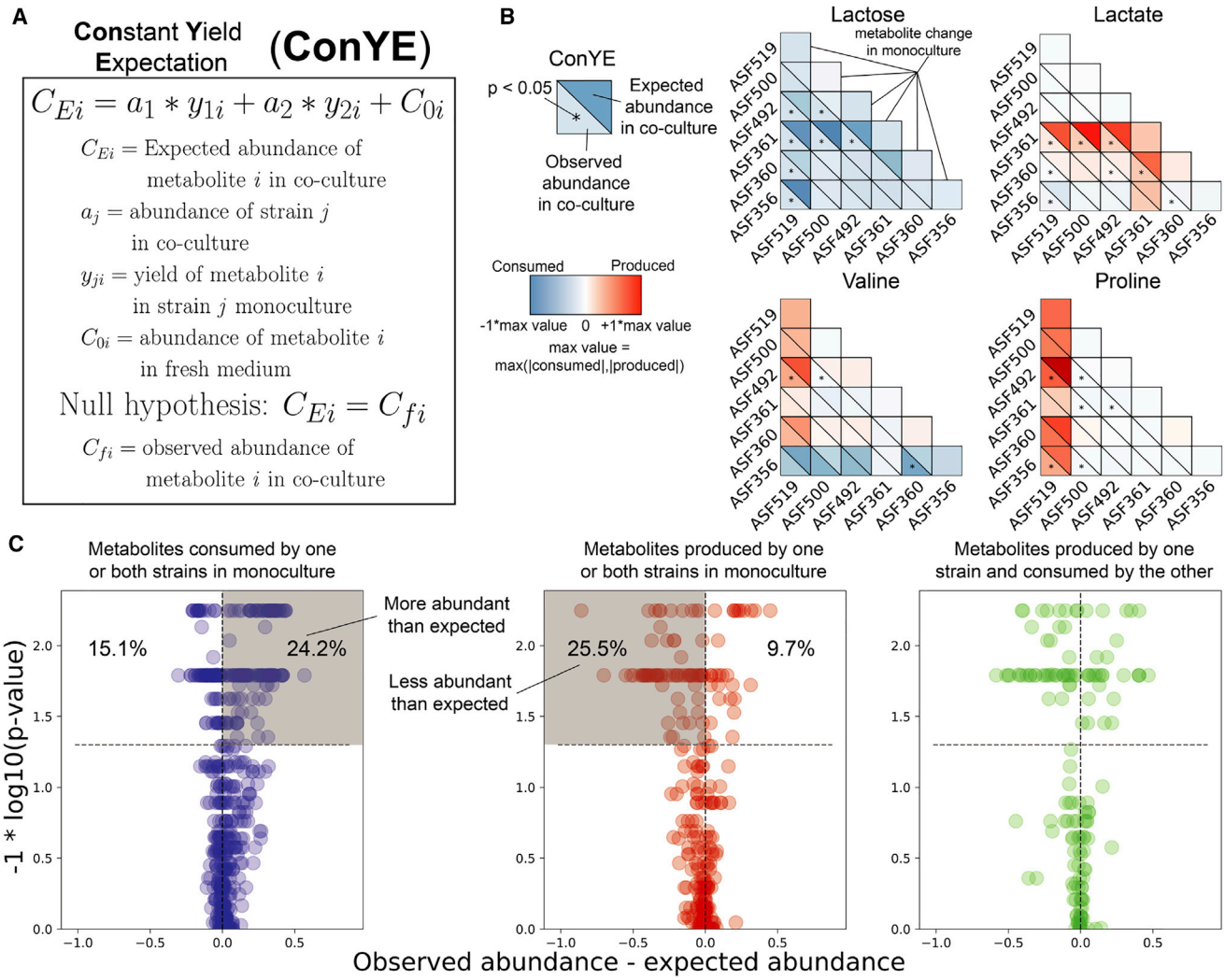

Figure 4. Accounting for Co-culture Growth Outcomes with ConYE to Identify Emergent Metabolism

(A) Procedure for the constant yield expectation (ConYE) model.

(B) Examples of ConYE results for lactose, lactate, valine, and proline. Diagonal shows monoculture behavior for each strain. Every pair of triangles indicates the observed metabolite abundance in co-culture (lower left), the expected metabolite abundance (upper right), and whether there was a significant difference between observed and expected values. Centering and scaling were performed as in Figure 3, except expected values were included while selecting a max value. Mann-Whitney U test with false discovery rate (FDR) control using the Benjamini-Hochberg procedure was performed for all 1,290 comparisons (15 co-cultures, 86 metabolites each). Asterisk indicates $p < 0.05$ for the metabolite in the co-culture containing the indicated strains.

(C) ConYE results for all strain pairings for metabolites that were consumed by one or both strains in monoculture (left, blue), produced by one or both strains in monoculture (middle, red), or produced by one strain in monoculture and consumed by the other strain in monoculture (right, green). Each point represents a metabolite in a co-culture pair. X axis shows the difference between observed and expected metabolite abundance in co-culture, scaled as in (B), and y axis shows the p value from ConYE. Points above the gray line have $p < 0.05$. Percentage of points in the labeled quadrant relative to the rest of the points in the subplot is shown.

Co-culture Increases the Efficiency of Metabolite Utilization

After applying ConYE to all co-cultures, the null hypothesis was rejected for 500 out of 1,290 metabolites (38.8%; 86 metabolites tested across 15 co-culture conditions, resulting in 1,290 comparisons), suggesting that co-culture alters the metabolism of a substantial portion of metabolites when taking into account changes in growth during co-culture. For metabolites that were consumed by one or both strains in monoculture, the amount consumed per unit of strain growth generally decreased in co-culture if the null hypothesis was rejected. Specifically, of the 624 instances of metabolites that fell into this category, 151 (24.2%) were significantly more abundant than expected in co-culture, whereas 94 (15.1%) were less abundant than expected (Figure 4C, left). Of the 278 instances of a metabolite being produced by one or both strains in a pairing in monoculture, 71 (25.5%) were less abundant than expected, while 27 (9.7%) were more abundant than expected (Figure 4C, middle). Thus, although co-culture often resulted in a greater quantity of a metabolite being produced relative to either monoculture (i.e.,

OPEN ACCESS
CellPress

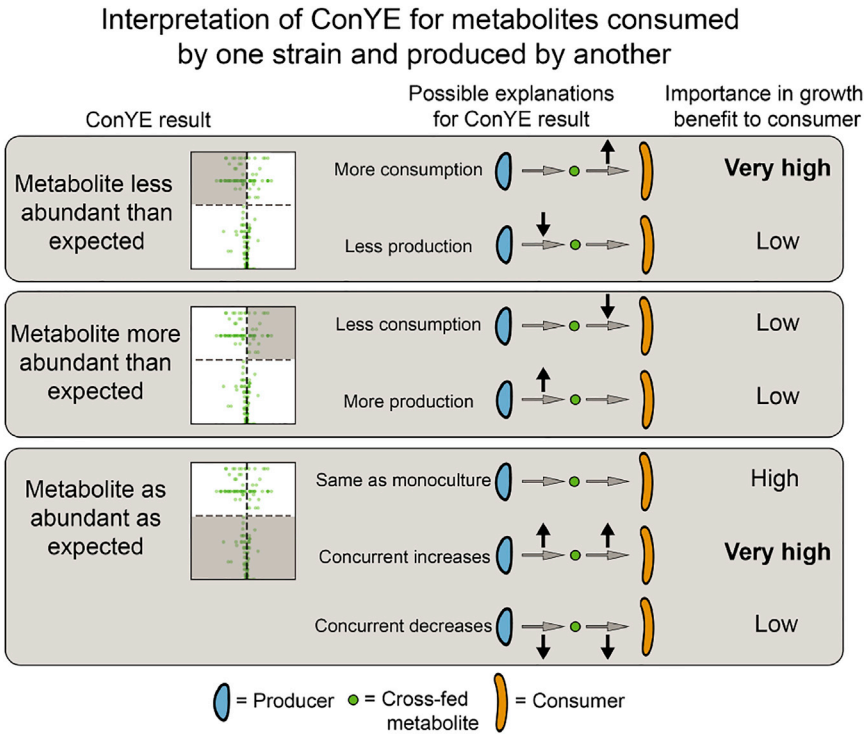

Figure 5. Interpretations of ConYE Results for Metabolites Consumed by One Strain in Monoculture and Produced by Another Strain in Monoculture

In this example, the consumer experienced a growth benefit. The shaded region of each volcano plot describes the points that fall into the category described on the left. In the "Importance in growth benefit to consumer" column, the entry for each scenario assumes that consumption of the metabolite is coupled with biomass production. The importance assignments are qualitative and reflect whether the consumer experienced an increase in metabolite flux in the explanatory scenario (high for increased flux, low for decreased flux).

metabolites driving monoculture and co-culture separation in PCA, Figure 3B), the amount produced relative to the growth of each strain decreased for most metabolites. Similarly, the amount of each metabolite consumed relative to biomass in co-culture generally decreased. These results suggest that these co-cultures can increase the efficiency of biomass production through niche expansion (e.g., consuming metabolites they did not consume in monoculture) or cross-feeding rather than increasing consumption of metabolites they did not fully deplete in monoculture. Indeed, 90 out of 1,290 (6.98%) metabolites were not consumed or produced by either strain in monoculture yet were consumed when the two strains were in co-culture.

These distinct ConYE trends are enriched in cases with positive growth interactions (Figure 6A). When considering only pairings with a positive growth effect for at least one strain, there were 219 metabolites that were consumed by one or both strains in monoculture. Of these 219 metabolites, 138 (63.0%) were more abundant than expected, while only 6 (2.74%) were less abundant than expected. Of the 88 metabolites produced by one or both strains in monoculture for these co-cultures, 51 (58.0%) were less abundant than expected, and only 5 (5.68%) were more abundant than expected. Taken together, these results indicate that co-cultures with positive interactions are able to more efficiently utilize resources than co-cultures without positive interactions or monocultures.

There are three mechanisms that may enable this phenotype: niche expansion (consumption of metabolites not consumed in monoculture), cross-feeding, and detoxification via consumption of growth-inhibiting metabolites. In co-culture, the subset of strain pairs with positive interactions consumed 30 metabolites that were not consumed by either species in monoculture. Interestingly, all 30 instances of emergent metabolite consumption were carried out by *Lactobacillus* ASF361+*Eubacterium* ASF492, *Lactobacillus* ASF361+*Pseudoflavonifractor* ASF500, and *Eubacterium* ASF492+*Parabacteroides* ASF519, while the remaining two pairs (*Clostridium* ASF356+*Parabacteroides* ASF519 and *Lactobacillus* ASF361+*Parabacteroides* ASF519) had 0 cases of emergent consumption (see Table S3 for all cases). Given this result, it is likely that the growth benefits that occurred for *Clostridium* ASF356+*Parabacteroides* ASF519 and *Lactobacillus* ASF361+*Parabacteroides* ASF519 are due to cross-feeding or detoxification, while the growth benefits for the other positive interaction pairs are at least in part due to niche expansion.

Identifying Cross-Fed Metabolites and Evaluating Feasibility *In Silico*

We next sought to investigate potential cross-fed metabolites from ConYE for co-cultures with positive growth interactions in order to find a mechanism that explained, at least in part, the growth benefit. For this task, we focused on the co-culture of *Clostridium* ASF356 and *Parabacteroides* ASF519 to exclude co-cultures that may have engaged in niche expansion (and therefore cross-feeding may have played a more minor role in observed growth benefits) and to remove the need to consider additional confounding factors introduced by a strong negative growth interaction (e.g., negative impact on *Parabacteroides* ASF519 growth in co-culture with *Lactobacillus* ASF361). Seven named metabolites were consumed by *Clostridium* ASF356 in monoculture that were also produced by *Parabacteroides* ASF519 in monoculture (Figure 6B; labeled metabolites satisfy criteria specified in figure caption). Of those seven metabolites, tyramine, valine, and choline did not result in rejecting the ConYE null hypothesis. Isoleucine and alanine were more abundant than expected, and proline and formate were less abundant than expected. Isoleucine and alanine may have been cross-fed, but, given that they were more abundant than expected, consumption of these metabolites only contributed to enhanced growth if *Parabacteroides* ASF519 also produced less of these metabolites than expected (as in middle inset of Figure 5, where

OPEN ACCESS
CellPress

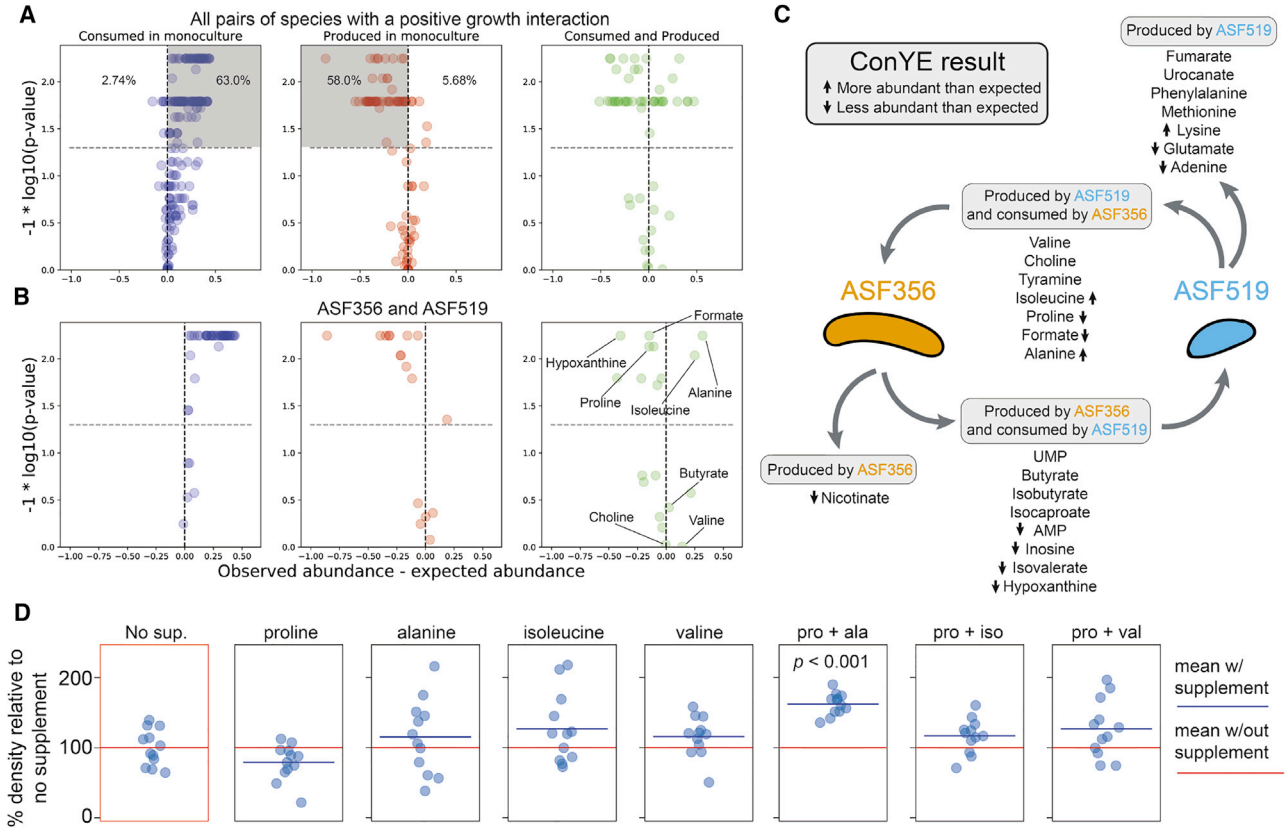

Figure 6. Emergent Metabolism in Co-culture Pairings with a Growth Benefit and *In Vitro* Testing

(A) ConYE results for all metabolites from co-cultures with a positive growth interaction. Shaded quadrants represent consumed metabolites that were more abundant than expected (left) or less abundant than expected (middle). Percentages shown represent the number of metabolites within the plot that fall in the quadrant.

(B) ConYE results for co-culture of *Clostridium* ASF356 and *Parabacteroides* ASF519. Metabolites on right for which $p > 0.05$ are labeled unless they could not be assigned an identity. Metabolites for which $p < 0.05$ are labeled if assigned an identity and abs(x) > 0.10 for that metabolite. X and y axes are scaled as in Figure 4.

(C) Metabolic interaction topology for *Clostridium* ASF356 and *Parabacteroides* ASF519. ConYE results are indicated with arrows pointing up or down for metabolites for which the null hypothesis was rejected. Metabolite classifications are based on monoculture behavior.

(D) OD600 of *Clostridium* ASF356 monocultures after 72 hr of growth in supplemented media conditions. "No sup." had no supplement added, while conditions with a single amino acid were supplemented at 1.25 g/L. In conditions with two supplements, each metabolite is supplemented at 1.25 g/L. "pro + ala," "pro + iso," and "pro + val" conditions include L-proline with L-alanine, L-isoleucine, or L-valine, respectively. Red line indicates mean OD600 in No sup condition, and blue line indicates mean OD600 in the labelled condition.

Parabacteroides ASF519 is the producer and *Clostridium* ASF356 is the consumer). Proline and formate were both less abundant than expected and so were either consumed by *Clostridium* ASF356 more in co-culture than in monoculture (and thereby cross-fed) or produced less by *Parabacteroides* ASF519 in co-culture than in monoculture (as in top inset of Figure 5).

ConYE can identify metabolites that are potentially cross-fed, but the actual behavior of each strain in co-culture with respect to that metabolite is difficult to infer using existing experimental techniques. Because we can only evaluate the co-culture behavior based on an expectation derived from monoculture behavior, it is still possible that co-culture leads to reduced production and consumption of those metabolites rather than cross-feeding. We sought to provide orthogonal evidence for ConYE results by evaluating the potential for metabolites to increase the growth rate of a strain in monoculture, reasoning that ConYE may produce false-positive inferences if metabolites are not actually coupled with biomass production. We chose to support inferences made using ConYE by building and applying genome-scale metabolic network reconstructions (GENREs). GENREs are mathematical representations of all metabolic reactions that an organism can carry out and have been used extensively to predict the effect of environmental conditions on the growth of bacterial species (Oberhardt et al., 2009). We created an ensemble of 100 GENREs for each strain in this study to gain greater confidence in cross-feeding predictions and to enable predictive modeling of metabolism in future studies (Figures S3A and S3B; see STAR Methods). For each metabolite, we evaluated its impact on the growth of individual strains by performing ensemble flux balance analysis (EnsembleFBA) (Biggs and Papin, 2017) to predict the growth rate of the strain without the metabolite available and with the metabolite available in excess (see STAR Methods). We performed this procedure for

the cross-feeding candidate metabolites between *Clostridium* ASF356 and *Parabacteroides* ASF519. If a metabolite increases the predicted *in silico* growth rate when available in excess, we take that as parallel evidence to support or oppose the ConYE-based inferences. EnsembleFBA results are summarized in Figure S3 for all metabolites except tyramine, which was not present in any GENREs within the ensemble for *Clostridium* ASF356.

Valine was essential for growth of *Clostridium* ASF356 in all 100 GENREs in its ensemble. Isoleucine was essential for 85 out of 100 GENREs but had no effect on growth for the other 15 GENREs, while the absence of the rest of the potentially cross-fed metabolites had no effect on the predicted growth rate. Given the *in silico* essentiality of valine and the ConYE results indicating valine was as abundant as expected, valine may have conferred a growth benefit to *Clostridium* ASF356 if cross-fed between *Clostridium* ASF356 and *Parabacteroides* ASF519. While isoleucine was essential for growth of the majority of GENREs in the *Clostridium* ASF356 ensemble, there was a subset of GENREs in which its removal had no effect. Given this *in silico* uncertainty, as well as the ConYE result that indicated it was more abundant than expected in co-culture, we hypothesized that cross-feeding of isoleucine may not have influenced the growth of *Clostridium* ASF356 as much as valine. Alanine, proline, choline, and formate were not essential and did not influence predicted growth rates *in silico*. Critically, however, this analysis indicated that availability of any of the individual metabolites in excess did not confer a growth benefit relative to the unsupplemented medium.

In Vitro Investigation of an Inferred Cross-Feeding Interaction

Given the lack of an *in silico* prediction that indicated that supplementation of a putatively cross-fed metabolite would increase the growth rate of *Clostridium* ASF356, we considered mechanisms through which the metabolites discussed above may interact with each other to influence growth, rather than in isolation as considered thus far. *Clostridium* ASF356 belongs to the genus *Clostridium*, throughout which amino acid fermentation via Stickland reactions is common (Mead, 1971). Stickland reactions involve coupling the oxidative deamination of one amino acid with the reductive decarboxylation of another amino acid, producing two short-chain fatty acids or branched chain fatty acids that each contain one fewer carbon than the respective amino acid from which they were derived (Nisman, 1954). Proline, glycine, hydroxyproline, and ornithine are strong Stickland reaction electron acceptors, while alanine, valine, leucine, and isoleucine are strong electron donors. We observed that *Clostridium* ASF356 consumed proline, a strong electron acceptor, and all the listed electron donors in monoculture, while *Parabacteroides* ASF519 produced proline, alanine, valine, and isoleucine and consumed leucine in monoculture. In co-culture, ConYE indicated that proline was significantly less abundant than expected, suggesting it was consumed more per unit biomass in co-culture than in monoculture. Given this observation and the lack of growth rate increase predicted *in silico* with excess proline available, we hypothesized that proline was of critical importance to the growth benefit for *Clostridium* ASF356 in co-culture with *Parabacteroides* ASF519 but depended on the presence of suitable electron donors. Behavior varied among the electron donors that may pair with proline in the Stickland reaction: isoleucine and alanine were more abundant than expected, while valine was as abundant as expected. The Stickland fermentation product for proline is 5-aminovalerate, which we could not identify within the NMR spectra due to spectral overlap with other metabolites and lack of signal in regions unique to 5-aminovalerate. The products for isoleucine, valine, and alanine are valeric acid (not detected), isobutyrate (as abundant as expected), and acetate (less abundant than expected), respectively. Decreased abundance of leucine, which is fermented to isovalerate (less abundant than expected), in co-culture suggests decreased consumption by *Clostridium* ASF356 or increased consumption of isovalerate by *Parabacteroides* ASF519, which consumed isovalerate in monoculture.

To test the hypothesis that *Clostridium* ASF356 experiences a growth benefit in the presence of proline and suitable electron donors, we grew *Clostridium* ASF356 in media supplemented with proline, alanine, isoleucine, valine, or each combination of the three electron donors (alanine, isoleucine, and valine) with proline. NMR spectroscopy cannot differentiate between amino acid isomers, so we assumed all amino acids consumed and produced were the L isoform (as in tryptone, the major source of amino acids in the medium). Organisms conducting Stickland fermentation of proline generally possess a proline racemase, since D-proline is the isoform that is fermented (Watanabe et al., 2015). Leucine was consumed by both strains in monoculture and thus was excluded because it was unlikely to be cross-fed in co-culture. Only the monoculture supplemented with both proline and alanine had increased density relative to no supplement (Figure 6D, $p < 0.05$, Mann-Whitney U test with false discovery rate control using the Benjamini-Hochberg procedure), suggesting that co-metabolism of proline and alanine contributes to the growth of *Clostridium* ASF356. Given that the ConYE results indicated that alanine was more abundant in co-culture than expected, the results of the supplementation experiment imply that production of alanine by *Parabacteroides* ASF519 was increased in co-culture with *Clostridium* ASF356 or that *Clostridium* ASF356 used alanine more efficiently in co-culture. Additionally, the lack of growth benefit conferred by supplementation of proline with isoleucine or valine suggests that any change attributable to pairing either electron donor with proline was too small to detect, given our sample size. Formate can also be used as an electron donor for proline reduction in the Stickland reaction (Kabisch et al., 1999), which we did not factor into our experiments. Formate was produced by *Parabacteroides* ASF519 and consumed by *Clostridium* ASF356 in monoculture and was less abundant than expected in co-culture according to ConYE. Thus, formate may have also contributed to the observed growth benefit.

After performing these supplementation experiments, we attempted identification of 5-aminovalerate in the supernatant from *Clostridium* ASF356 and *Parabacteroides* ASF519 co-culture using 2D ^{1}H homonuclear correlation spectroscopy (COSY), which can identify metabolites with overlap in 1D NMR spectra (Figure S5; STAR Methods). 5-aminovalerate was not present at detectable quantities; the peaks within the overlapping region which we suspected to contain 5-aminovalerate were from valine and gamma-aminobutyrate (GABA). Thus,

Please cite this article in press as: Medlock et al., Inferring Metabolic Mechanisms of Interaction within a Defined Gut Microbiota, Cell Systems (2018), https://doi.org/10.1016/j.cels.2018.08.003

Stickland fermentation occurred only if 5-aminovalerate was further degraded. Such activity has been observed in *Clostridium viride* (formerly *Clostridium aminovalericum*), which converts 5-aminovalerate to valerate, acetate, propionate, and ammonia (Barker, 1985; Barker et al., 1987). Additionally, synthesis of GABA from glutamate is broadly distributed in plants and bacteria, and the responsible enzyme in some organisms is known to convert 5-aminovalerate to glutamate via promiscuous 5-aminovalerate transaminase activity (Shin et al., 2016; Yonaha et al., 1985). Both *Clostridium* ASF356 and *Parabacteroides* ASF519 have multiple putative proteins similar to known 5-aminovalerate transaminase enzymes (BLAST E value < 1E-50, 31%–34% identity; compared to the *gabT* gene from *Pseudomonas putida* KT2440), so either strain may be capable of producing GABA from 5-aminovalerate.

We also tested the effect of concurrent supplementation with Stickland pairs *in silico*, which did not lead to any predicted growth benefit because the GENREs do not contain Stickland fermentation reactions. Stickland reactions are absent from reaction databases used to construct and curate GENREs such as the ModelSEED biochemistry database (Henry et al., 2010) but are present in the AGORA resource of semi-automatically generated GENREs for gut microbes (Magnúsdóttir et al., 2017). None of the genes involved in Stickland fermentation have been identified in the genome of *Clostridium* ASF356 as of this writing (determined via searching the annotated *Clostridium* ASF356 genome in PATRIC (Wattam et al., 2017), BLAST against D-proline reductase gene subunits). Taken together, these results suggest that proline and alanine co-supplementation confers a growth benefit through an alternative pathway or through Stickland fermentation with the subsequent breakdown of 5-aminovalerate.

DISCUSSION

In this study, we used data-driven methods to identify metabolic signatures that may contribute to growth modulation in bacterial co-cultures, proposed mechanisms by which a specific signature may arise, and verified that growth of the benefiting strain is enhanced when putatively cross-fed metabolites are supplemented *in vitro*. The biochemical capability we evaluated experimentally, Stickland fermentation of proline and alanine, is widely distributed in proteolytic *Clostridia* (Mead, 1971). While the ability of species inhabiting the mammalian gut to perform Stickland fermentation has been investigated, this study connects possible Stickland fermentation to a metabolic interspecies interaction that modulates growth. Given that some of the end products of Stickland fermentation were present at low concentrations in the fresh medium and that *Parabacteroides* ASF519 consumed them in monoculture (isobutyrate, isovalerate, and isocaproate), our data suggest that this interaction may be bidirectional. This observation supports some theoretical motifs for metabolism in the gastrointestinal tract proposed in the literature, such as the model of carbon and nitrogen flow proposed by Fischbach and Sonnenburg, in which *Clostridia* (e.g., *Clostridium* ASF356) ferment amino acids, providing ammonium and other amino acid fermentation products to *Bacteroides* (e.g., *Parabacteroides* ASF519, which was assigned to the genus *Bacteroides* prior to 2006) (Fischbach and Sonnenburg, 2011; Sakamoto and Benno, 2006). *Clostridium* ASF356 and *Parabacteroides* ASF519 are co-located along the mouse gastrointestinal tract; however, the relevance of this observation is unclear given a microbiota as restricted in size as the ASF (Sarma-Rupavtarm et al., 2004). This kind of interaction has direct relevance to enteric pathogens as emerging evidence indicates that *in vivo* utilization of proline via Stickland fermentation is highly active in *C. difficile* during sustained infection in mice (Fletcher et al., 2018; Jenior et al., 2017, 2018).

We expect that the growth outcome observed in the co-culture of *Clostridium* ASF356 and *Parabacteroides* ASF519 is due to a multitude of interactions that each have a small effect. An alternative mechanism by which co-culture could enhance growth is consumption of growth-inhibiting metabolite products. Although we did not explore them in this study, ConYE identified several cases in which this process may have occurred. For example, in the co-culture of *Lactobacillus* ASF361 and *Parabacteroides* ASF519, lactate, hypoxanthine, AMP, and uridine monophosphate (UMP) were all metabolites produced by *Lactobacillus* ASF361 and consumed by *Parabacteroides* ASF519 that were less abundant than expected in co-culture. Of these metabolites, lactate is known to have potent antimicrobial properties both broadly and against *Lactobacillus spp.* (Shelef, 1994); thus, it is a reasonable candidate for this mechanism.

We developed ConYE to interrogate growth-modulating interactions within this study, but the framework can be used to study interspecies interactions that alter other phenotypes of interest. For example, the same analyses conducted here could be performed using consumption of a substrate of interest, such as lactose, to calculate metabolite yields as a function of that substrate rather than as a function of strain abundance. In this scenario, ConYE could be used to identify co-culture pairings that enhance conversion of lactose to a metabolite of interest and to identify cross-fed metabolites that contribute to an enhanced yield of that metabolite of interest.

There is increasing interest in developing methods for inference of growth or abundance-modulating interactions between microbes from various data types and environments (Friedman et al., 2017; Weiss et al., 2016; Xiao et al., 2017). These methods have primarily been focused on discovering interspecies interactions and the role they might play in ecosystem function, rather than ascribing mechanism to those interactions. Interspecies interactions are likely to be highly context dependent, so more detailed knowledge about mechanisms of interaction is necessary to generalize these findings (Chamberlain et al., 2014). Several approaches that integrate the metabolic and/or spatial environment using genome-scale metabolic models have been developed that account for context dependency (Chan et al., 2017; Harcombe et al., 2014; Zomorrodi and Maranas, 2012). However, limitations in biochemical knowledge across the bacterial tree of life limit their broad application to other organisms. Large-scale efforts to collect and assimilate biochemical knowledge of gut microbes within genome-scale metabolic models are in progress, but experimental data to validate and improve the predictive ability of these models are lacking (Magnúsdóttir et al., 2017). Recent work to determine defined growth conditions for gut microbes will accelerate the process of experimental validation for such models, but data are still extremely sparse relative to organisms for which highly predictive

metabolic models have been developed (Tramontano et al., 2018). Similar metabolic model-based approaches have been applied to simplified versions of communities such as the human gut microbiota (Bauer et al., 2017; Chan et al., 2017), but the poor experimental tractability of these systems makes testing predicted interspecies interactions challenging, and thus they are left unvalidated.

Incorporating dynamic substrate utilization information may be able to provide more accurate insight into metabolic interactions than the method we present. We envision that our method may be used as an efficient screening step in which many species are grown across many media conditions to identify putative interactions. Then, in conditions with many putative interactions, sampling can be performed with finer time resolution to attain a clearer picture of the actual coupling of metabolite consumption and production with changes in growth of individual species, as previously performed with yeast and lactic acid bacteria (Ponomarova et al., 2017). This framework and others that model substrate utilization within a microbial community over time could be modified with the strain abundance normalization procedure used within ConYE to identify dynamic features of emergent metabolic behavior in these communities (Erbilgin et al., 2017).

We have developed an experimental and computational pipeline to probe interspecies interactions and infer putative metabolic mechanisms of interaction, generating testable hypotheses. Understanding mechanisms of interspecies interaction and the environmental conditions that induce them is a prerequisite to engineering communities with specific therapeutic or industrial value. For generalizable methods that predict interspecies interaction using mechanistic models to be successful, methods must be validated experimentally. This task will require a substantially larger set of observed interspecies interactions than are presented here or are available in the literature, from which to derive generalizable principles. Extending our approach and similar methods to defined communities across conditions that are more diverse, both in terms of resource availability and spatial structure, will begin to make predictive modeling of interspecies interactions tractable.

STAR★METHODS

Detailed methods are provided in the online version of this paper and include the following:

- KEY RESOURCES TABLE
- CONTACT FOR REAGENT AND RESOURCE SHARING
- EXPERIMENTAL MODEL AND SUBJECT DETAILS
  - Strain Maintenance
- METHOD DETAILS
  - Media Formulation
  - *In Vitro* Monoculture and Co-culture Growth Experiments in 12-Well plates
  - *In Vitro* Amino Acid Supplementation Experiments
  - DNA Extraction
  - Hydrolysis Probe-Based qPCR Assay Design
  - Monoculture and Co-culture Growth Curve Experiments
  - ^{1}H Nuclear Magnetic Resonance Spectroscopy-Based Metabolomics
- QUANTIFICATION AND STATISTICAL ANALYSIS
  - Differential Abundance Testing
  - Principal Component Analysis
  - Constant Yield Expectation Model
  - Draft Genome-Scale Metabolic Network Reconstruction and Analysis
  - Metabolomics-Constrained Gapfilling
  - Metabolomics-Constrained Gapfilling Algorithm
  - GENRE Quality Control
  - *In Silico* Simulations
- DATA AND SOFTWARE AVAILABILITY

SUPPLEMENTAL INFORMATION

Supplemental Information includes five figures and three tables and can be found with this article online at https://doi.org/10.1016/j.cels.2018.08.003.

ACKNOWLEDGMENTS

We acknowledge the University of Virginia ARCS staff for providing assistance in setting up software used for gapfilling on the UVA computing cluster. We thank Jie Liu for helpful guidance on hydrolysis probe design for qPCR and Thomas Moutinho for experimental assistance performing sample extraction. We thank all members of the Papin lab for helpful project feedback. We acknowledge funding from the National Institutes of Health R01GM108501, T32LM012416, and T32GM008136.

AUTHOR CONTRIBUTIONS

Conceptualization, G.L.M., M.A.C., J.R.S., G.L.K., and J.A.P.; Data Curation, G.L.M. and G.L.K.; Formal Analysis, G.L.M.; Investigation, G.L.M., M.A.C., D.G.M., M.B.M., N.G., J.R.S., and G.L.K.; Methodology, G.L.M.; Software, G.L.M. and J.R.S.; Validation, G.L.M., M.A.C., and G.L.K.; Visualization, G.L.M. and J.R.S.; Writing – Original Draft, G.L.M.; Writing – Review & Editing, G.L.M., M.A.C., D.G.M., M.B.M., N.G., J.R.S., G.L.K., and J.A.P.; Funding Acquisition, J.R.S., G.L.K., and J.A.P.; Project Administration, J.R.S., G.L.K., and J.A.P.; Resources, J.R.S., G.L.K., and J.A.P.; Supervision, J.R.S., G.L.K., and J.A.P.

DECLARATION OF INTERESTS

The authors declare no competing interests.

Received: February 8, 2018
Revised: June 15, 2018
Accepted: August 3, 2018
Published: September 5, 2018

REFERENCES

Barker, H.A. (1985). Pathway of 5-aminovalerate degradation by Clostridium aminovalericum. Curr. Top Cell Regul. *26*, 349–354.

Barker, H.A., D'Ari, L., and Kahn, J. (1987). Enzymatic reactions in the degradation of 5-aminovalerate by Clostridium aminovalericum. J. Biol. Chem. *262*, 8994–9003.

Bauer, E., Zimmermann, J., Baldini, F., Thiele, I., and Kaleta, C. (2017). BacArena: individual-based metabolic modeling of heterogeneous microbes in complex communities. PLoS Comput. Biol. *13*, e1005544.

Beckonert, O., Keun, H.C., Ebbels, T.M.D., Bundy, J., Holmes, E., Lindon, J.C., and Nicholson, J.K. (2007). Metabolic profiling, metabolomic and metabonomic procedures for NMR spectroscopy of urine, plasma, serum and tissue extracts. Nat. Protoc. *2*, 2692–2703.

Benedict, M.N., Mundy, M.B., Henry, C.S., Chia, N., and Price, N.D. (2014). Likelihood-based gene annotations for gap filling and quality assessment in genome-scale metabolic models. PLoS Comput. Biol. *10*, e1003882.

Benjamini, Y., and Hochberg, Y. (1995). Controlling the false discovery rate: A practical and powerful approach to multiple testing. J. R. Stat. Soc. Series B Stat. Methodol. *57*, 289–300.

Biggs, M.B., and Papin, J.A. (2017). Managing uncertainty in metabolic network structure and improving predictions using EnsembleFBA. PLoS Comput. Biol. *13*, e1005413.

Biggs, M.B., Medlock, G.L., Moutinho, T.J., Lees, H.J., Swann, J.R., Kolling, G.L., and Papin, J.A. (2017). Systems-level metabolism of the altered Schaedler flora, a complete gut microbiota. ISME J. *11*, 426–438.

Britton, R.A., and Young, V.B. (2014). Role of the intestinal microbiota in resistance to colonization by Clostridium difficile. Gastroenterology *146*, 1547–1553.

Brugiroux, S., Beutler, M., Pfann, C., Garzetti, D., Ruscheweyh, H.J., Ring, D., Diehl, M., Herp, S., Lötscher, Y., Hussain, S., et al. (2016). Genome-guided design of a defined mouse microbiota that confers colonization resistance against Salmonella enterica serovar Typhimurium. Nat. Microbiol. *2*, 16215.

Buffie, C.G., and Pamer, E.G. (2013). Microbiota-mediated colonization resistance against intestinal pathogens. Nat. Rev. Immunol. *13*, 790–801.

Chamberlain, S.A., Bronstein, J.L., and Rudgers, J.A. (2014). How context dependent are species interactions? Ecol. Lett. *17*, 881–890.

Chan, S.H.J., Simons, M.N., and Maranas, C.D. (2017). SteadyCom: predicting microbial abundances while ensuring community stability. PLoS Comput. Biol. *13*, e1005539.

Dewhirst, F.E., Chien, C.C., Paster, B.J., Ericson, R.L., Orcutt, R.P., Schauer, D.B., and Fox, J.G. (1999). Phylogeny of the defined murine microbiota: altered Schaedler flora. Appl. Environ. Microbiol. *65*, 3287–3292.

Dona, A.C., Jiménez, B., Schäfer, H., Humpfer, E., Spraul, M., Lewis, M.R., Pearce, J.T.M., Holmes, E., Lindon, J.C., and Nicholson, J.K. (2014). Precision high-throughput proton NMR spectroscopy of human urine, serum, and plasma for large-scale metabolic phenotyping. Anal. Chem. *86*, 9887–9894.

Ebrahim, A., Lerman, J.A., Palsson, B.O., and Hyduke, D.R. (2013). COBRApy: COnstraints-based reconstruction and analysis for Python. BMC Syst. Biol. *7*, 74.

Erbilgin, O., Bowen, B.P., Kosina, S.M., Jenkins, S., Lau, R.K., and Northen, T.R. (2017). Dynamic substrate preferences predict metabolic properties of a simple microbial consortium. BMC Bioinformatics *18*, 57.

Fischbach, M.A., and Sonnenburg, J.L. (2011). Eating for two: how metabolism establishes interspecies interactions in the gut. Cell Host Microbe *10*, 336–347.

Fletcher, J.R., Erwin, S., Lanzas, C., and Theriot, C.M. (2018). Shifts in the gut metabolome and clostridium difficile transcriptome throughout colonization and infection in a mouse model. mSphere *3*, https://doi.org/10.1128/mSphere.00089-18.

Friedman, J., Higgins, L.M., and Gore, J. (2017). Community structure follows simple assembly rules in microbial microcosms. Nat. Ecol. Evol. *1*, 109.

Geuking, M.B., Cahenzli, J., Lawson, M.A.E., Ng, D.C.K., Slack, E., Hapfelmeier, S., McCoy, K.D., and Macpherson, A.J. (2011). Intestinal bacterial colonization induces mutualistic regulatory T cell responses. Immunity *34*, 794–806.

Gillis, C.C., Hughes, E.R., Spiga, L., Winter, M.G., Zhu, W., Furtado de Carvalho, T., Chanin, R.B., Behrendt, C.L., Hooper, L.V., Santos, R.L., et al. (2018). Dysbiosis-associated change in host metabolism generates lactate to support Salmonella growth. Cell Host Microbe *23*, 54–64.e6.

Goldford, J.E., Lu, N., Bajić, D., Estrela, S., Tikhonov, M., Sanchez-Gorostiaga, A., Segrè, D., Mehta, P., and Sanchez, A. (2018). Emergent simplicity in microbial community assembly. Science *361*, 469–474.

Harcombe, W.R., Riehl, W.J., Dukovski, I., Granger, B.R., Betts, A., Lang, A.H., Bonilla, G., Kar, A., Leiby, N., Mehta, P., et al. (2014). Metabolic resource allocation in individual microbes determines ecosystem interactions and spatial dynamics. Cell Rep. *7*, 1104–1115.

Harp, J.A., Chen, W., and Harmsen, A.G. (1992). Resistance of severe combined immunodeficient mice to infection with Cryptosporidium parvum: the importance of intestinal microflora. Infect. Immun. *60*, 3509–3512.

Henry, C.S., DeJongh, M., Best, A.A., Frybarger, P.M., Linsay, B., and Stevens, R.L. (2010). High-throughput generation, optimization and analysis of genome-scale metabolic models. Nat. Biotechnol. *28*, 977–982.

Holland, P.M., Abramson, R.D., Watson, R., and Gelfand, D.H. (1991). Detection of specific polymerase chain reaction product by utilizing the 5'−−3'exonuclease activity of Thermus aquaticus DNA polymerase. Proc. Natl. Acad. Sci. USA *88*, 7276–7280.

Ivanov, I.I., Atarashi, K., Manel, N., Brodie, E.L., Shima, T., Karaoz, U., Wei, D., Goldfarb, K.C., Santee, C.A., Lynch, S.V., et al. (2009). Induction of intestinal Th17 cells by segmented filamentous bacteria. Cell *139*, 485–498.

Jenior, M.L., Leslie, J.L., Young, V.B., and Schloss, P.D. (2017). Clostridium difficile colonizes alternative nutrient niches during infection across distinct murine gut microbiomes. mSystems *2*, https://doi.org/10.1128/mSystems.00063-17.

Jenior, M.L., Leslie, J.L., Young, V.B., and Schloss, P.D. (2018). Clostridium difficile alters the structure and metabolism of distinct cecal microbiomes during initial infection to promote sustained colonization. mSphere *3*, https://doi.org/10.1128/mSphere.00261-18.

Jensen, P.A., Dougherty, B.V., Moutinho, T.J., Jr., and Papin, J.A. (2015). Miniaturized plate readers for low-cost, high-throughput phenotypic screening. J. Lab. Autom. *20*, 51–55.

Kabisch, U.C., Gräntzdörffer, A., Schierhorn, A., Rücknagel, K.P., Andreesen, J.R., and Pich, A. (1999). Identification of d-proline reductase from Clostridium sticklandii as a selenoenzyme and indications for a catalytically active pyruvoyl group derived from a cysteine residue by cleavage of a proprotein. J. Biol. Chem. *274*, 8445–8454.

Kale, N.S., Haug, K., Conesa, P., Jayseelan, K., Moreno, P., Rocca-Serra, P., Nainala, V.C., Spicer, R.A., Williams, M., Li, X., et al. (2016). MetaboLights: an open-access database repository for metabolomics data. Curr. Protoc. Bioinformatics *53*, 14.13.1-18.

Kluyver, T., Ragan-Kelley, B., Pérez, F., Granger, B.E., Bussonnier, M., Frederic, J., Kelley, K., Hamrick, J.B., Grout, J., Corlay, S., et al. (2016). Jupyter Notebooks-a publishing format for reproducible computational workflows. In Positioning and Power in Academic Publishing: Players, Agents and Agendas, F. Loizides and B. Schmidt, eds. (IOS Press), pp. 87–90.

Lawley, T.D., and Walker, A.W. (2013). Intestinal colonization resistance. Immunology *138*, 1–11.

Louis, P., and Flint, H.J. (2009). Diversity, metabolism and microbial ecology of butyrate-producing bacteria from the human large intestine. FEMS Microbiol. Lett. *294*, 1–8.

Magnúsdóttir, S., Heinken, A., Kutt, L., Ravcheev, D.A., Bauer, E., Noronha, A., Greenhalgh, K., Jäger, C., Baginska, J., Wilmes, P., et al. (2017). Generation of genome-scale metabolic reconstructions for 773 members of the human gut microbiota. Nat. Biotechnol. *35*, 81–89.

Mead, G.C. (1971). The amino acid-fermenting clostridia. J. Gen. Microbiol. *67*, 47–56.

Momeni, B., Xie, L., and Shou, W. (2017). Lotka-Volterra pairwise modeling fails to capture diverse pairwise microbial interactions. Elife *6*, https://doi.org/10.7554/eLife.25051.

Muir, M., Williams, L., and Ferenci, T. (1985). Influence of transport energization on the growth yield of Escherichia coli. J. Bacteriol. *163*, 1237–1242.

Nisman, B. (1954). The Stickland reaction. Bacteriol. Rev. *18*, 16–42.

Oberhardt, M.A., Palsson, B.Ø., and Papin, J.A. (2009). Applications of genome-scale metabolic reconstructions. Mol. Syst. Biol. *5*, 320.

Pedregosa, F., Varoquaux, G., Gramfort, A., Michel, V., Thirion, B., Grisel, O., Blondel, M., Prettenhofer, P., Weiss, R., Dubourg, V., et al. (2011). Scikit-learn: machine learning in Python. J. Mach. Learn. Res. *12*, 2825–2830.

Ponomarova, O., Gabrielli, N., Sévin, D.C., Mülleder, M., Zirngibl, K., Bulyha, K., Andrejev, S., Kafkia, E., Typas, A., Sauer, U., et al. (2017). Yeast creates a niche for symbiotic lactic acid bacteria through nitrogen overflow. Cell Syst. *5*, 345–357.e6.

Rakoff-Nahoum, S., Coyne, M.J., and Comstock, L.E. (2014). An ecological network of polysaccharide utilization among human intestinal symbionts. Curr. Biol. *24*, 40–49.

Reed, J.L., Patel, T.R., Chen, K.H., Joyce, A.R., Applebee, M.K., Herring, C.D., Bui, O.T., Knight, E.M., Fong, S.S., and Palsson, B.O. (2006). Systems approach to refining genome annotation. Proc. Natl. Acad. Sci. USA *103*, 17480–17484.

Reichardt, N., Duncan, S.H., Young, P., Belenguer, A., McWilliam Leitch, C., Scott, K.P., Flint, H.J., and Louis, P. (2014). Phylogenetic distribution of three pathways for propionate production within the human gut microbiota. ISME J. *8*, 1323–1335.

Royston, J.P. (1982). Algorithm AS 181: the W test for normality. J. R. Stat. Soc. Ser. C Appl. Stat. *31*, 176–180.

Sakamoto, M., and Benno, Y. (2006). Reclassification of Bacteroides distasonis, Bacteroides goldsteinii and Bacteroides merdae as Parabacteroides distasonis gen. nov., comb. nov., Parabacteroides goldsteinii comb. nov. and Parabacteroides merdae comb. nov. Int. J. Syst. Evol. Microbiol. *56*, 1599–1605.

Sarma-Rupavtarm, R.B., Ge, Z., Schauer, D.B., Fox, J.G., and Polz, M.F. (2004). Spatial distribution and stability of the eight microbial species of the altered schaedler flora in the mouse gastrointestinal tract. Appl. Environ. Microbiol. *70*, 2791–2800.

Schwan, C., Stecher, B., Tzivelekidis, T., van Ham, M., Rohde, M., Hardt, W.D., Wehland, J., and Aktories, K. (2009). Clostridium difficile toxin CDT induces formation of microtubule-based protrusions and increases adherence of bacteria. PLOS Pathog. *5*, e1000626.

Sezonov, G., Joseleau-Petit, D., and D'Ari, R. (2007). Escherichia coli physiology in Luria-Bertani broth. J. Bacteriol. *189*, 8746–8749.

Shelef, L.A. (1994). Antimicrobial effects of lactates: a review. J. Food Prot. *57*, 445–450.

Shin, J.H., Park, S.H., Oh, Y.H., Choi, J.W., Lee, M.H., Cho, J.S., Jeong, K.J., Joo, J.C., Yu, J., Park, S.J., et al. (2016). Metabolic engineering of Corynebacterium glutamicum for enhanced production of 5-aminovaleric acid. Microb. Cell Fact. *15*, 174.

Sievers, F., Wilm, A., Dineen, D., Gibson, T.J., Karplus, K., Li, W., Lopez, R., McWilliam, H., Remmert, M., Söding, J., et al. (2011). Fast, scalable generation of high-quality protein multiple sequence alignments using clustal omega. Mol. Syst. Biol. *7*, 539.

Singer, S.M., and Nash, T.E. (2000). The role of normal flora in Giardia lamblia infections in mice. J. Infect. Dis. *181*, 1510–1512.

Song, Y., Liu, C., Lee, J., Bolanos, M., Vaisanen, M.L., and Finegold, S.M. (2005). "Bacteroides goldsteinii sp. nov." isolated from clinical specimens of human intestinal origin. J. Clin. Microbiol. *43*, 4522–4527.

Stecher, B., and Hardt, W.D. (2008). The role of microbiota in infectious disease. Trends Microbiol. *16*, 107–114.

Tramontano, M., Andrejev, S., Pruteanu, M., Klünemann, M., Kuhn, M., Galardini, M., Jouhten, P., Zelezniak, A., Zeller, G., Bork, P., et al. (2018). Nutritional preferences of human gut bacteria reveal their metabolic idiosyncrasies. Nat. Microbiol. *3*, 514–522.

Turnbaugh, P.J., Ley, R.E., Hamady, M., Fraser-Liggett, C.M., Knight, R., and Gordon, J.I. (2007). The human microbiome project. Nature *449*, 804–810.

Veselkov, K.A., Lindon, J.C., Ebbels, T.M.D., Crockford, D., Volynkin, V.V., Holmes, E., Davies, D.B., and Nicholson, J.K. (2009). Recursive segment-wise peak alignment of Biological (1)h NMR spectra for improved metabolic biomarker recovery. Anal. Chem. *81*, 56–66.

Vos, P., Garrity, G., Jones, D., Krieg, N.R., Ludwig, W., Rainey, F.A., Schleifer, K.-H., and Whitman, W.B. (2011). Bergey's manual of systematic bacteriology. In The Firmicutes, *Volume 3* (Springer Science & Business Media), pp. 466–467.

Wannemuehler, M.J., Overstreet, A.M., Ward, D.V., and Phillips, G.J. (2014). Draft genome sequences of the altered schaedler flora, a defined bacterial community from gnotobiotic mice. Genome Announc. *2*, https://doi.org/10.1128/genomeA.00287-14.

Watanabe, S., Tanimoto, Y., Nishiwaki, H., and Watanabe, Y. (2015). Identification and characterization of bifunctional proline racemase/hydroxyproline epimerase from archaea: discrimination of substrates and molecular evolution. PLoS One *10*, e0120349.

Wattam, A.R., Davis, J.J., Assaf, R., Boisvert, S., Brettin, T., Bun, C., Conrad, N., Dietrich, E.M., Disz, T., Gabbard, J.L., et al. (2017). Improvements to PATRIC, the all-bacterial bioinformatics database and analysis resource center. Nucleic Acids Res. *45*, D535–DD542.

Weiss, S., Van Treuren, W., Lozupone, C., Faust, K., Friedman, J., Deng, Y., Xia, L.C., Xu, Z.Z., Ursell, L., Alm, E.J., et al. (2016). Correlation detection strategies in microbial data sets vary widely in sensitivity and precision. ISME J. *10*, 1669–1681.

Wilkins, T.D., Fulghum, R.S., and Wilkins, J.H. (1974). Eubacteriurm plexicaudatum sp. nov., an anaerobic bacterium with a subpolar tuft of flagella, isolated from a mouse cecum. Int.J. Syst. Bacteriol. *24*, 408–411.

Wymore Brand, M., Wannemuehler, M.J., Phillips, G.J., Proctor, A., Overstreet, A.M., Jergens, A.E., Orcutt, R.P., and Fox, J.G. (2015). The altered Schaedler flora: continued applications of a defined murine microbial community. ILAR J. *56*, 169–178.

Xiao, Y., Angulo, M.T., Friedman, J., Waldor, M.K., Weiss, S.T., and Liu, Y.Y. (2017). Mapping the ecological networks of microbial communities. Nat. Commun. *8*, 2042.

Ye, J., Coulouris, G., Zaretskaya, I., Cutcutache, I., Rozen, S., and Madden, T.L. (2012). Primer-BLAST: a tool to design target-specific primers for polymerase chain reaction. BMC Bioinformatics *13*, 134.

Yonaha, K., Suzuki, K., and Toyama, S. (1985). 4-aminobutyrate: 2-oxoglutarate aminotransferase of Streptomyces griseus: purification and properties. Eur. J. Biochem. *146*, 101–106.

Zomorrodi, A.R., and Maranas, C.D. (2012). OptCom: a multi-level optimization framework for the metabolic modeling and analysis of microbial communities. PLoS Comput. Biol. *8*, e1002363.

Please cite this article in press as: Medlock et al., Inferring Metabolic Mechanisms of Interaction within a Defined Gut Microbiota, Cell Systems (2018), https://doi.org/10.1016/j.cels.2018.08.003

STAR★METHODS

KEY RESOURCES TABLE

REAGENT or RESOURCE	SOURCE	IDENTIFIER
Bacterial and Virus Strains		
Clostridium sp. ASF356	Gift from Michael Wannemuehler & Gregory Phillips	N/A
Lactobacillus intestinalis ASF360	Gift from Michael Wannemuehler & Gregory Phillips	N/A
Lactobacillus murinus ASF361	Gift from Michael Wannemuehler & Gregory Phillips	N/A
Eubacterium plexicaudatum ASF492	Gift from Michael Wannemuehler & Gregory Phillips	N/A
Pseudoflavonifractor sp. ASF500	Gift from Michael Wannemuehler & Gregory Phillips	N/A
Parabacteroides goldsteinii ASF519	Gift from Michael Wannemuehler & Gregory Phillips	N/A
Chemicals, Peptides, and Recombinant Proteins		
probe fluorophores and quenchers	See Table S1	N/A
Primer and probe synthesis	Integrated DNA Technologies	N/A
PerfeCTa MultiPlex qPCR ToughMix (5X)	Quantabio	Cat# 95147
ASL buffer (Qiamp stool kit)	Qiagen	Cat# 19082
DeNovix dsDNA quantification kit	DeNovix	Cat# KIT-DSDNA-BROAD-2
Deposited Data		
Metabolomics	Metabolights database	MTBLS705
All raw data, processed data, and results	https://github.com/gregmedlock/asf_interactions	N/A
Primers and probes	This paper, see Table S1	N/A
Software and Algorithms		
ConYE	This paper, https://github.com/gregmedlock/asf_interactions	N/A
Medusa	https://github.com/gregmedlock/medusa	N/A
All other code associated with manuscript	https://github.com/gregmedlock/asf_interactions	N/A

CONTACT FOR REAGENT AND RESOURCE SHARING

Further information and requests for resources and reagents should be directed to and will be fulfilled by the Lead Contact, Jason Papin (papin@virginia.edu).

EXPERIMENTAL MODEL AND SUBJECT DETAILS

Strain Maintenance

All strains are identified within the manuscript by their genus followed by the original isolate designation numbers for the ASF, and solely by their designation numbers within figures. Formal designations as shown in Figure 1B are as follows: *Clostridium sp. ASF356*, *Lactobacillus intestinalis ASF360*, *Lactobacillus murinus ASF361*, *Eubacterium plexicaudatum ASF492*, *Pseudoflavonifractor sp. ASF500*, and *Parabacteroides goldsteinii ASF519*. *Mucispirillum schaedleri ASF457* was excluded from the study due to lack of detectable growth in the experimental medium, and *Clostridium sp. ASF502* was excluded due to inconsistent growth in the experimental medium. Stock vials for all ASF strains were maintained at -80°C in 50% glycerol, 50% brain-heart infusion (BHI) medium (see media formulations for the composition of brain-heart infusion media used in this study). All strains were grown in an anaerobic chamber (Shellab BACTRONEZ, Sheldon Manufacturing, Inc., Cornelius, Oregon, USA) filled with mixed anaerobic gas

(5% CO_2, 5% H_2, 90% N_2). Anaerobic conditions were ensured through the use of palladium catalysts (baked at 120°C when outside the chamber and rotated daily when first entering the chamber) and anaerobic indicator strips (Oxoid, Basingstoke, UK).

METHOD DETAILS

Media Formulation

Supplemented Brain–Heart Infusion medium, referred to as BHI throughout the manuscript: Brain–Heart Infusion base (37 g/L, BD, Franklin Lakes, NJ, USA), supplemented with yeast extract (5 g/L), 0.2 mL of vitamin K1 solution (0.5% vitamin K1 dissolved in 99.5% ethanol), 0.5 mL/L of hemin solution (0.5 g/L dissolved in 1% NaOH, 99% deionized water), L-cysteine (0.5 g/L) and 5m L/L each of newborn calf serum, horse serum, and sheep serum. Vitamin K1, hemin, and all sera were added after autoclaving the medium. For preparation of agar plates, agar was supplemented at 12g/L.

Modified Lennox LB medium, referred to as mLB throughout the manuscript: 30 g/L LB base in powder form (Sigma, St Louis, MO, USA) was combined with 0.376g/L L-cysteine (Sigma), 39mL of a mineral salts solution (containing 6 g/L KH_2PO_4, 6 g/L $(NH_4)_2SO4$, 12g/L NaCl, 2.5g/L $MgSO_4 \cdot 7H_2O$, 1.6 g/L $CaCl_2 \cdot 2H_2O$, all dissolved in deionized water), 15 mL/L of hemin solution (0.5 g/L dissolved in 1% NaOH, 99% deionized water), 0.3 mL of vitamin K1 solution (0.5% vitamin K1 dissolved in 99.5% ethanol), 15m L/L of lactose solution (5g/L lactose dissolved in deionized water) and 15 mL/L of tween 20 solution (1 g/L tween 20 dissolved in deionized water).

All supplements that were made using deionized water, or those that could not be autoclaved, were filter-sterilized using a 0.22μm membrane (except the sera).

In Vitro Monoculture and Co-culture Growth Experiments in 12-Well plates

Strains were inoculated from frozen stock to grow a dense lawn on agar plates containing BHI media. Prior to inoculation, all agar plates were equilibrated inside an anaerobic chamber for at least 24 hours. Inoculated plates were incubated for 3-9 days before being used to start overnight cultures. For overnight cultures, 50 mL of mLB broth in a 500 mL glass flask was inoculated using a generous streak from the lawn of each strain, then each flask was covered with a Breathe-Easy membrane (Diversified Biotech, Dedham, Massachusetts, USA). After 18-24 hours of incubation at 37°C, overnight cultures were transferred to 50 mL conical tubes, sealed, transferred out of the chamber, and centrifuged at 15,000 xg for 5 minutes. After centrifugation, samples were transferred into the chamber, supernatant was poured off, and pellets were resuspended in 12.7 mL mLB broth. The resuspension for each species was then diluted to make inoculant with the same concentration of cells as a solution at an optical density of 0.01, measured at OD600 with 100uL of sample volume in a flat-bottom 96-well plate (with a well diameter of 0.64 cm) using a Tecan infinite m200 plate reader (Tecan Group Ltd., Männedorf, Switzerland). This final inoculant was then used to inoculate mLB broth in 12-well plates. For monoculture samples, 100μL of inoculant was added to 2.9 mL of media. For co-culture samples, 100μL of each strain's inoculant was added to 2.8 mL of media. 12-well plates were covered with a Breathe-Easy membrane, then the 12-well plate lid was placed on top of the membrane. Inoculated, covered 12-well plates were incubated at 37°C for 72 hours.

After 72 hours of incubation, 12-well plates were removed from the incubator and membranes were opened for each well using a razor. For each well, the sample was mixed by pipetting 900μL three times, then 1.8 mL of sample was transferred to a 2 mL snap-cap tube. 200μL of sample was also collected after mixing and transferred to a 96-well plate to measure optical density at OD600. Samples within 2 mL tubes were then transferred out of the chamber and centrifuged at 18,407 xg for 2 minutes. After centrifugation, supernatant was poured directly into a 3 mL syringe attached to a syringe pump filter (0.22 μm pore size, mixed cellulose ester filter) and filtered into a 2 mL snap-cap tube. Cell pellets were then resuspended in 400μL Qiagen lysis buffer (Buffer ASL, Qiagen) and vortexed until thoroughly mixed. Resuspended pellets and spent media were then frozen at -80°C.

To ensure reproducibility, 3 experiments were performed in which independent overnight starter cultures were used to inoculate 3 samples per monoculture and co-culture condition (resulting in 9 total replicates). For the third experiment, *Eubacterium* ASF492 and *Pseudoflavonifractor* ASF500 did not appear to grow in monoculture as measured by both OD600 and qPCR, and their metabolomes did not appear significantly different than any negative controls, so all sample groups containing *Eubacterium* ASF492 and *Pseudoflavonifractor* ASF500 in the third experiment were excluded from analyses. As a result, those sample groups have N = 6 replicates throughout the study.

In Vitro Amino Acid Supplementation Experiments

Inoculant for *Clostridium* ASF356 was prepared as described for monoculture and co-culture experiments in 12-well plates. Solutions of amino acids in deionized water were filter-sterilized (0.22 μm pore size) and transferred to the anaerobic chamber and allowed to equilibrate for one week. Equilibrated solutions were mixed with liquid mLB broth (prepared as described previously), generating solutions that contained 90% mLB and 10% supplement by volume. Final concentrations were 1.25g/L for single amino acid supplements and 1.25g/L of each of two amino acids for supplements containing two amino acids (i.e. individual amino acids are at the same concentration in supplements containing one or two amino acids). 96-well plates were filled with 193μL media and 7μL inoculant (approximately the same initial density as in 12-well experiments), covered with a Breathe-Easy membrane, then incubated at 37°C for 72 hours. After incubation, the 96-well plates were removed from the anaerobic chamber, the breatheasy membrane was peeled off each plate, and the OD600 was measured in the 96 well plate.

Please cite this article in press as: Medlock et al., Inferring Metabolic Mechanisms of Interaction within a Defined Gut Microbiota, Cell Systems (2018), https://doi.org/10.1016/j.cels.2018.08.003

DNA Extraction

Zirconia beads (1mm; BioSpec Products) were added to samples in ASL buffer (QIAmp Stool kit), and samples disrupted using a Mini-Beadbeater (15s, two times), followed by heat treatment (5 min, 90°C, 800 rpm; Eppendorf Thermomixer). Debris was pelleted (14,000 xg, 1 min), and 400μL transferred to a QIAcube rotor adapter. Total DNA from each sample isolated on the QIAcube using the 'human stool' protocol provided by the manufacturer and stored at -20°C prior to PCR. Purified DNA used for standards in PCR assays was quantified using the DeNovix dsDNA kit. DNA standards were adjusted to 2ng/μL and diluted 10-fold to generate standard curves in PCR assays.

Hydrolysis Probe-Based qPCR Assay Design

4-plex (including *Clostridium* ASF356, *Eubacterium* ASF492, *Clostridium* ASF502, and *Parabacteroides* ASF519) and 3-plex (*Lactobacillus* ASF360, *Lactobacillus* ASF361, and *Pseudoflavonifractor* ASF500) hydrolysis probe-based quantitative polymerase chain reaction (qPCR) assays were designed to quantify the abundance of each strain's DNA with high specificity and throughput (Holland et al., 1991). Probe and primer design began with the *groEL* gene, which encodes the highly-conserved molecular chaperone GroEL, as a putative target. The National Center for Biotechnology Information PrimerBLAST web interface was used to identify PCR targets for each strain with minimal sequence similarity with any region in another strain's genome (Ye et al., 2012). PCR products ranging from 70-200 base pairs with a calculated melting temperature between 57°C and 63°C were determined, requiring at least two mismatches with unintended targets, with at least two mismatches occurring within the last five base pairs at the 3' end. We screened the top three primer pairs for each strain returned by PrimerBLAST for sensitivity and specificity using standard SYBR green chemistry, and determined that all primers for *Lactobacillus* ASF360, *Lactobacillus* ASF361, and *Pseudoflavonifractor* ASF500 had poor sensitivity. To identify alternative PCR products for *Lactobacillus* ASF360, *Lactobacillus* ASF361, and *Pseudoflavonifractor* ASF500, we performed BLAST for each putative gene in each strain against all other putative genes in ASF strains. For genes with no off-target hits (E-value > 1.0 for all comparisons), we attempted primer design using PrimerBLAST until a gene was found for each strain with at least 4 suitable primer pairs. All 4 primer pairs for the remaining ASF strains were screened for specificity and sensitivity and at least one suitable primer pair was found for each strain.

For all 7 strains in the qPCR assays, probes were then designed for each primer pair. The 7 strains were split into a 3-plex and 4-plex reaction based on typical density observed experimentally, with strains growing to higher densities in the 4-plex reaction and strains growing to lower densities in the 3-plex reaction. For each probe in each reaction, we performed multiple sequence alignment using Clustal Omega (Sievers et al., 2011). Suitable probe sequences were identified manually according to five criteria: 1) maximize the number of mismatches at the 5' end of the probe, 2) probe length between 20-30 base pairs, 3) estimated melting temperature around 66-70°C, 4) 35-65% GC content, and 5) no G or C at the 5' end of the probe. Final primers, products, probe sequences, and accompanying probe fluorophores and quenchers are provided in Table S1. Since only relative comparisons within each strain are made, the effects of non-single copy genes do not confound the data.

Primers and probes were synthesized by Integrated DNA Technologies, Inc. (Coralville, Iowa, USA). PerfeCTa 5X MultiPlex qPCR ToughMix (Quantabio, Beverly, MA) was used for all reactions. Each PCR reaction (20μL total volume) contained ToughMix (1X concentration), 300 nM of each forward primer, 300nM of each reverse primer, and 100 nM of each probe, with 4μL of DNA sample. The optimal cycling conditions were determined to be: initial denaturation of 3 min at 95°C followed by 40 cycles of 15s at 95°C and 30s at 61°C. All assays achieved an efficiency between 91.4% and 100.5%, except for Cy5 quantification in the first and third of 3 total 96-well plates used in the study. These assays achieved an efficiency of 124.4% and 138.8%, respectively. Efficiency was calculated using a diluted DNA standard (10-fold dilution starting with 2 ng/μL down to 0.002 ng/μL) for each strain created using purified genomic DNA. Each PCR plate contained independent standard curves. Reactions were run using the BioRad CFX Touch, and analyzed using the software provided (where Cq value is equated to DNA concentration based on the standard curve).

Throughout the manuscript, qPCR data are presented as abundance values for each strain, which are z-score normalized using the mean monoculture abundance to center the data (i.e. mean value from each strain's monoculture corresponds to a z-score of 0) and the standard deviation of monoculture abundance to scale the data. Thus, the z-score for the abundance of a strain can be compared across any condition. Abundance of every strain was quantified in all samples (including negative controls), and cross-contamination was not detected in any sample.

Monoculture and Co-culture Growth Curve Experiments

Inoculant was prepared as described for 12-well experiments, wells were inoculated using the same starting cell density as used in 12-well experiments, and identical growth conditions were used. Optical density was measured at 589 nm using a miniaturized plate reader (Jensen et al., 2015). Experiments were performed in 96 well plates with 200uL total volume in each well and a breatheasy membrane. Each sample group (monocultures and co-cultures) contains 8 biological replicates from a single experiment (e.g. each replicate was grown in an independent well, but they were derived from the same starter culture). After 72 hours, samples were removed from the anaerobic chamber, the breatheasy membrane was removed, and the endpoint optical density was recorded in a Tecan Infinite m200 plate reader (Tecan Group Ltd, Männedorf, Switzerland) at OD600. This endpoint optical density was used to linearly scale the values from the miniaturized plate reader. Raw and scaled growth curve data are available in the GitHub repository accompanying the paper.

^{1}H Nuclear Magnetic Resonance Spectroscopy-Based Metabolomics

Samples were prepared for ^{1}H NMR spectroscopy as described by Dona et al. (2014). Samples were thawed at room temperature and centrifuged at 12,000 xg at 4°C for 10 minutes, before 540 μl of supernatant was combined with 60 μl of buffer (pH 7.4; 1.5 mM KH2PO4, 0.1% TSP (3-(trimethylsilyl)propionic- 2,2,3,3-d4 acid sodium salt) in 100% D2O) and transferred to a SampleJet NMR tube (Bruker BioSpin, Rheinstetten, Germany). Standard one-dimensional (1D) ^{1}H-NMR spectra with water pre-saturation were acquired at 300 K using a 600 MHz Avance III spectrometer (Bruker), equipped with a SampleJet autosampler (Bruker). A total of 32 scans were collected into 64,000 data points for each sample. Spectra were automatically phased, baseline corrected and calibrated to the TSP resonance at δ^1H 0 in Topspin 3.1 software (Bruker). The spectra were imported into MATLAB R2014a (The Mathworks, Inc., Natick, MA, USA). Biologically irrelevant regions of the spectra were removed (TSP resonance at δ^1H 0 and residual water peak δ ^{1}H 4.5- 5.2) before peak alignment by recursive segment-wise peak alignment (RSPA) (Veselkov et al., 2009). The loadings of pairwise principal component analysis models, as well as manual comparisons between fresh media spectra and spent media of each bacterial strain, were used to assign metabolite identities to peaks. To further identify metabolites that may only have been produced or consumed in co-culture, group means for all 15 co-culture conditions were compared to fresh media across the entire spectra. The relevant regions of the spectra were integrated to calculate relative spectral intensities for each metabolite. Metabolite identities were assigned by reference to known spectra in multiple databases. For all analyses, integrals were centered by subtracting the mean value for each metabolite in the blank samples, then scaled by the maximum absolute value of all centered values (so that the minimum and maximum possible scaled values for each metabolite were -1 and +1, respectively). We assume that concentration is proportional to the integrated peak area for each metabolite across all samples, thus relative concentrations can be inferred for each metabolite across all samples. After 72 hours of growth in this medium, pH ranges from 5.48-6.55 for these strains, thus only minor pH-dependent effects may be present in the spectra. The peak integral values, scaled values, peak integration regions and identities, and associated R code for analysis and visualization is available in the GitHub repository. Raw spectra are available in the Metabolights database under identifier MTBLS705 (Kale et al., 2016).

Additional two-dimensional (2D) NMR experiments (^{1}H-^{1}H correlation spectroscopy [COSY]) were performed on a selected sample of supernatant from co-culture of *Clostridium* ASF356 and *Parabacteroides* ASF519 to assist with metabolite identification (Beckonert et al., 2007). For these experiments a total of 512 increments with 4 scans were acquired into 2,000 data points with a spectral width of 12 ppm for each dimension.

QUANTIFICATION AND STATISTICAL ANALYSIS

Differential Abundance Testing

DNA quantification data for each sample group (each strain in monoculture and each unique co-culture condition) were tested for normality using the Shapiro-Wilk test (implemented via the shapiro.test function in R version 3.4.2) (Royston, 1982). The data for all but one monoculture sample groups were normally distributed, but the majority of co-culture sample groups were non-normally distributed, so the non-parametric Mann-Whitney *U*-test was chosen to test for differential DNA abundance. The same procedure was performed for the metabolomic data, and the majority of sample groups and metabolites were found to be non-normally distributed, so the Mann-Whitney *U*-test was performed to test for differential metabolite abundance as well, identifying metabolites as either produced, consumed, or unchanged based on testing results and the value of the group mean relative to the fresh media. For tests of differential abundance, the false discovery rate (FDR) was controlled using the Benjamini-Hochberg procedure (Benjamini and Hochberg, 1995). For DNA differential abundance testing, the number of sample groups used for FDR control was 21 (6 monocultures and 15 co-cultures). For metabolite differential abundance testing, the number of sample groups used for FDR control was 1,806 (21 mono- and co-culture groups, each with 86 integrated metabolite peaks that were tested for differential abundance against fresh media samples). The results of all normality and differential abundance testing, and notebooks performing the calculations, are available in the GitHub repository accompanying this work.

Principal Component Analysis

Principal component analysis (PCA) was performed on integrated peak values using the PCA function implemented in sci-kit learn (v0.19.2) in python v3.6 (Pedregosa et al., 2011).

Constant Yield Expectation Model

For each sample group, metabolite integrals were centered by subtracting the mean value of the metabolite integral in fresh medium (i.e. negative control). Centered integrals were then scaled by the max of the absolute values across all sample groups for each metabolite, resulting in values for each metabolite being scaled between -1 and +1, with at least one sample group taking a value of -1 or +1 for each metabolite. For each monoculture sample group, the mean of each scaled, centered metabolite was then divided by the mean DNA abundance of the corresponding strain, resulting in a metabolite yield specifying the amount of increase or decrease of a metabolite per unit of DNA for each strain. For each co-culture sample, the expected concentration of each metabolite was determined by multiplying the abundance of each strain in co-culture by the monoculture-derived yield, summing the two quantities from each strain, then subtracting the concentration of the metabolite in the fresh medium using the mean across negative controls (N=9). Using the calculated expected concentration from all samples within a co-culture group, deviation from expectation was determined by comparing expected concentrations to the observed concentrations in co-culture. Differential abundance was

Please cite this article in press as: Medlock et al., Inferring Metabolic Mechanisms of Interaction within a Defined Gut Microbiota, Cell Systems (2018), https://doi.org/10.1016/j.cels.2018.08.003

determined using the Mann-Whitney *U*-test with FDR control via the Benjamini-Hochberg procedure (Benjamini and Hochberg, 1995) and the mean of differences between expected and observed concentrations was recorded. The sample size used for FDR control was 1,290 (15 co-culture groups, each compared to a simulated constant yield expectation [ConYE] value for each of 86 metabolites). We explored the effect of variation in metabolite yields by leave-two-out bootstrap sampling of monocultures when performing the average yield calculation, followed by completion of the rest of ConYE for each subsample, and did not find that the results of significance testing were influenced by this subsampling (Figure S4). Jupyter notebooks performing the calculations for ConYE, the results of all tests, and the exploration of yield bootstrapping are available in the GitHub repository accompanying this work.

Draft Genome-Scale Metabolic Network Reconstruction and Analysis

Draft genome-scale metabolic network reconstructions (GENREs) were generated for *Clostridium* ASF356, *Lactobacillus* ASF360, *Lactobacillus* ASF361, *Eubacterium* ASF492, *Pseudoflavonifractor* ASF500, *Clostridium* ASF502 (not evaluated experimentally in the present study), and *Parabacteroides* ASF519 using a local installation of ProbModelSEED (Benedict et al., 2014; Henry et al., 2010). Draft genome sequences for the strains from the same experimental stock used in this study were used as input to ProbModelSEED (Wannemuehler et al., 2014). Briefly, ProbModelSEED annotates the genome for each organism to identify metabolic functions associated with genes or sets of genes. This process results in a draft GENRE containing high-confidence reactions for each species. To enable biomass production in the GENRE, gapfilling is performed with uptake enabled for any metabolite with a transporter annotated in the draft GENRE (i.e. simulating a rich medium). The resulting GENRE contains the original reactions associated with the organism's annotated genome, as well as non-gene associated reactions added to enable biomass production. ProbModelSEED also assigns reaction probabilities to each reaction that can be added during gapfilling, which are derived using sequence similarity for genes which did not meet the similarity threshold for annotation via RAST, or reactions for which portions of a complex were not detected. These probabilities are incorporated during gapfilling, leading to preferential addition of reactions for which there was some genetic evidence.

Metabolomics-Constrained Gapfilling

After generation of draft GENREs, we added functionality to the GENREs using a previously-generated supernatant metabolomics dataset in which the same ASF strains were grown in the same medium used in this study (Biggs et al., 2017). Using the original metabolite annotations for the dataset, we constrained the GENRE for each ASF strain by forcing production and consumption of any metabolite with a z-score normalized abundance of > +1 or < -1, respectively. Z-scores from the publication from which the data were drawn were used. This constraint was enforced by setting the lower bound of the exchange reaction for produced metabolites to 0.001 mmol/(g dry weight * hour), and the upper bound for exchange reactions for consumed metabolites to -0.001 mmol/(g dry weight * hour). The value of the constraint (0.001 mmol/(g dry weight * hour)) was chosen to be arbitrarily low, since absolute changes in metabolite concentrations were not derived in the metabolomics dataset used for gapfilling. Then, we set the remaining boundary conditions for each GENRE to represent the medium in which they were grown (as described in the *in silico* simulations section), and forced arbitrarily low flux through the biomass reaction (0.005/hour). Then, we checked for transporters for each metabolite for each strain that enabled import (for consumed metabolites) and export (for produced metabolites). If a suitable transport reaction was not present, we added a transporter from the ModelSEED biochemistry database and constrained the directionality to be as observed (e.g. import only for consumed metabolites, export only for produced metabolites). Transporter assignments are provided in Table S2. We then performed gapfilling using a modified version of the SMILEY algorithm (Reed et al., 2006) as implemented in Cobrapy v0.5.11. See "Metabolomics-Constrained Gapfilling" for exact algorithmic details. We used the set of all ProbModelSEED reactions for which reaction probabilities were assigned as the universal reactions for gapfilling, but excluded reactions containing O_2. We weighed the penalty for addition of each of these reactions by 1 - p, where p is the reaction probability, which ranges from 0 for unlikely reactions to 1 for highly likely reactions. The effect of this penalty is that high-probability reactions are assigned lower penalties, and are thus more likely to be added to the GENRE during gapfilling. For each ASF strain, metabolomics-constrained gapfilling was performed 10 times, each for 10 iterations, resulting in an ensemble of 100 GENREs. All 100 GENREs for each strain were unique (i.e. none of the iterations resulted in identical reaction sets being added to the draft GENRE).

Metabolomics-Constrained Gapfilling Algorithm

Metabolomics-constrained gapfilling was performed to ensure the GENRE for each species could produce biomass in the *in vitro* medium and produce and consume metabolites as determined by supernatant metabolomics. We used a modified version of the growmatch algorithm (Reed et al., 2006) with variable reaction penalties calculated in ProbModelSEED (Benedict et al., 2014). We implemented and applied the modified version of our algorithm in cobrapy v0.5.11 using the Gurobi solver v7.0 (Gurobi Optimization, Beaverton, Oregon) (Ebrahim et al., 2013). The algorithm is formally defined as:

$$\text{Min} \sum (c_j a_j) \;\; \textit{for } j \in [0, 1, \; \ldots \# \textit{universal reactions}], \text{ subject to:}$$

$$S \cdot v + U \cdot y = 0,$$

$$v_{biomass} > 0.005\ hr^{-1},$$

$$v_{lb,i} < v_i < v_{ub,i},$$

$$a_j y_{min,j} < y_j < a_j y_{max,j}\ ,\ a \in \{0,1\},$$

$$0.001 < v_k < v_{ub,k}\ \ for\ k \in Exchange\ reactions\ for\ produced\ metabolites,$$

$$v_{lb,g} < v_g < -0.001 for\ g \in Exchange\ reactions\ for\ consumed\ metabolites,$$

where $c = 1 - p$ and is the reaction cost associated with including each reaction from the universal reaction bag, p is the probability of each reaction (derived from sequence information using ProbModelSEED; reactions not assigned a probability receive a probability of 0) and a is the integer indicator for each reaction j in the universal reaction bag used during gapfilling (here, we use the ModelSEED biochemistry database). S is the stoichiometric matrix, v is the vector of fluxes through each reaction represented in the stoichiometric matrix, U is the universal reaction bag, y is the vector of fluxes through reactions in the universal reaction bag (which is multiplied by the integer a to force flux to take a zero or non-zero value), $v_{biomass}$ is flux through the biomass reaction (which we constrain to take a minimum value of 0.005 hr^{-1} to force an arbitrarily low, non-zero amount of growth), v_k are the fluxes through exchange reactions for metabolites that were designated as produced, v_g are the fluxes through exchange reactions for metabolites that were designated as consumed, and i is the index for each reaction within the GENRE. v_{lb}, the lower bound of flux through a reaction, was 0 for irreversible reactions and -1000 for reversible reactions. v_{ub}, the upper bound of flux through a reaction, was 1,000 for all reactions. v_{lb} for exchange reactions were set to -1000 for all metabolites detected in the medium by NMR spectroscopy and 0 for metabolites not detected.

We performed gapfilling for 10 independent runs for each species, in which each run had 10 dependent iterations that each generate a solution containing a set of reactions that, when added to the GENRE and activated, satisfy the constraints (i.e., all metabolites can be produced and consumed as indicated, and biomass can be produced). Within each run, the penalty for each reaction was increased by setting $c = 2c$ to encourage unique solutions. For reactions in the ModelSEED biochemistry that did not receive probabilities because they have no associated gene (e.g. spontaneous reactions), we set $c = 100$ to discourage addition of these reactions unless they were essential for any solution to be found. After each of 10 independent runs, reaction penalties were reset to their original value prior to beginning the next run. We reduced the integrality threshold in cobrapy to 1E-8 from the original value of 1E-6, because the default setting returned many solutions that did not satisfy the constraints applied due to numerical error for *Lactobacillus* ASF361 (e.g. the reaction list returned did not enable biomass production for this species because reactions from the universal reaction bag had values for y that were below 1E-6; decreasing the integrality threshold properly returned these reactions and enabled biomass production). For every ASF strain, all 100 GENREs constructed were unique.

GENRE Quality Control

All GENREs within the ensemble for each strain were assessed for mass balance. To perform this assessment, an intracellular demand reaction was added for each metabolite in the GENRE, and all exchange reactions were closed. Flux through each demand reaction was then optimized iteratively, and demand reactions that could carry flux indicated presence of a mass-imbalanced reaction that allowed spontaneous generation of the metabolite. This process identified three reactions in the draft GENREs that were mass-imbalanced (SEED ids: rxn15543 in *Parabacteroides* ASF519 GENRE; rxn33894 and rxn30984 in *Lactobacillus* ASF361). These reactions were removed from the draft GENREs, and the metabolomics-constrained gapfilling process was repeated using the draft GENREs with the reactions removed. These reactions have been removed from the ModelSEED biochemistry database since the generation of these draft GENREs.

All GENREs within the ensemble for each strain were also assessed for infeasible ATP production. Using boundary conditions that mimic the *in vitro* medium (as in in *silico* simulations, below), we optimized flux through an ATP demand reaction, and found that all GENREs for all strains generated between 0.5 and 1.9 mmol ATP/(g dry weight * hour). Normalizing this value by the uptake of lactose, which was 0.22 mmol/(g dry weight * hour) for all strains, gives a yield range of 2.27-8.64 units of ATP per unit of lactose, within reason for anaerobic organisms (for example, *Escherichia coli* is known to produce 2.2-3.2 units of ATP per unit of glucose when grown anaerobically) (Muir et al., 1985). Although erroneous energy generating cycles may be present in the GENREs presented here, the realistic ATP yield determined for all GENREs suggests they are unlikely to influence simulation results in this media condition.

In Silico Simulations

Flux balance analysis (FBA) was performed using version 0.8.1 of the cobrapy package and the Gurobi solver v7.0 (Ebrahim et al., 2013). Ensembles of GENREs were analyzed using Cobrapy methods through the Medusa package (G.L.M. and J.A.P., unpublished, https://github.com/gregmedlock/Medusa/). Media composition was determined by calculating exact concentrations for defined supplements (Hemin, Vitamin K1, Lactose, Tween-20), and a concentration of 1 mM was assumed to allow an uptake rate of 1 mmol/(g dry weight * hour). For media components with approximately known concentrations in LB (amino acids), the uptake rate was set to 5 mmol/(g dry weight * hour) based on a concentration of around 5 mM for most amino acids in LB

Please cite this article in press as: Medlock et al., Inferring Metabolic Mechanisms of Interaction within a Defined Gut Microbiota, Cell Systems (2018), https://doi.org/10.1016/j.cels.2018.08.003

(Sezonov et al., 2007). For components detected via metabolomics that were not amino acids or supplemented, and therefore likely originated from the yeast extract in LB, the maximal uptake rate was set to 0.1 mmol/(g dry weight * hour). For *in silico* media supplements and knockouts, a metabolite was considered essential if removal of the metabolite from the *in silico* medium caused the flux through biomass to fall below 1E-5/hour (used because of limits of numerical precision for the solvers used; use of a lower threshold (1E-10/hr) does not affect these results).

DATA AND SOFTWARE AVAILABILITY

All raw and processed data and all code used in this project except software used to process raw NMR spectra are available at https://github.com/gregmedlock/asf_interactions. Where possible, Jupyter notebooks (Kluyver et al., 2016) are used for reproducibility and to display results alongside corresponding analyses. The raw NMR spectra have been deposited in Metabolights under MTBLS705.

Cell Systems, Volume 7

Supplemental Information

Inferring Metabolic Mechanisms of Interaction within a Defined Gut Microbiota

Gregory L. Medlock, Maureen A. Carey, Dennis G. McDuffie, Michael B. Mundy, Natasa Giallourou, Jonathan R. Swann, Glynis L. Kolling, and Jason A. Papin

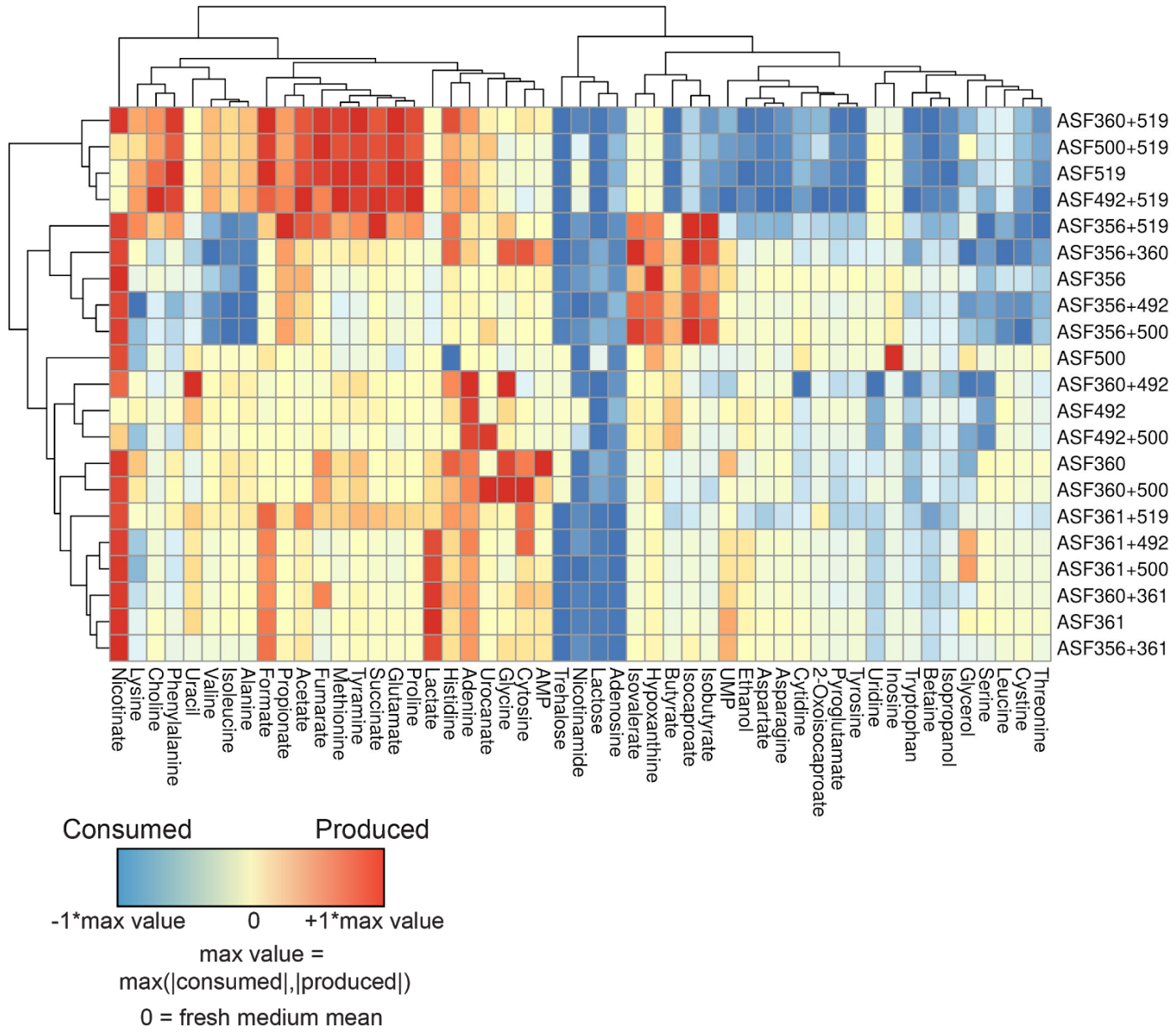

Figure S1. Heatmap describing supernatant metabolomes for all mono- and co-cultures after growth (related to Figure 3). Red indicates higher concentration than fresh medium, while blue indicates lower concentration. Values are centered at 0 using the mean value in fresh media, then scaled between -1 and +1 by dividing by the maximum change in concentration for each metabolite in any sample in the study. Only metabolites for which an identity could be determined are shown. Hierarchical clustering of metabolites was performed using Euclidean distances and complete linkage.

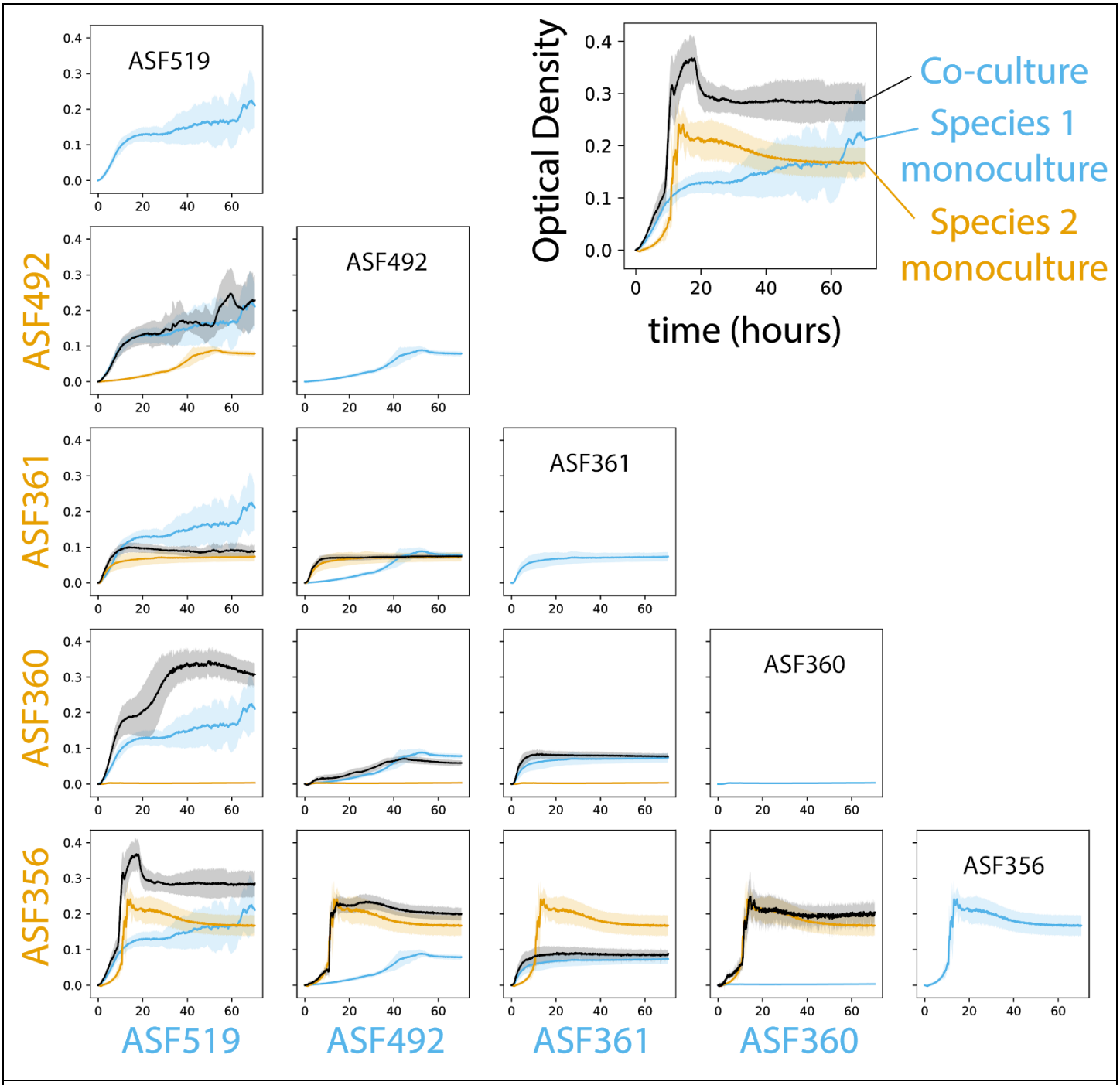

Figure S2. Optical density-based growth curves for *Clostridium* ASF356, *Lactobacillus* ASF360, *Lactobacillus* ASF361, *Eubacterium* ASF492, and *Parabacteroides* ASF519 (related to Figures 1 and 2). Optical density was measured at 589nm. Experiments were performed in 96 well plates with 200uL total volume in each well. Each sample group (monocultures and co-cultures) contains 8 biological replicates from a single experiment (e.g. each replicate was grown in an independent well, but they were derived from the same starter culture). Line shows the mean for each sample group, and shading extends one standard deviation from the mean in both the positive and negative direction. Sky blue line indicates monoculture for the strain labelled in sky blue along the x axis. Orange line indicates monoculture for the strain labelled in orange along the y axis. Black line indicates co-culture of the two strains. Diagonal shows the monoculture growth curve for each species. Axes units are identical on all subplots. Time is shown in hours, extending to 72 hours.

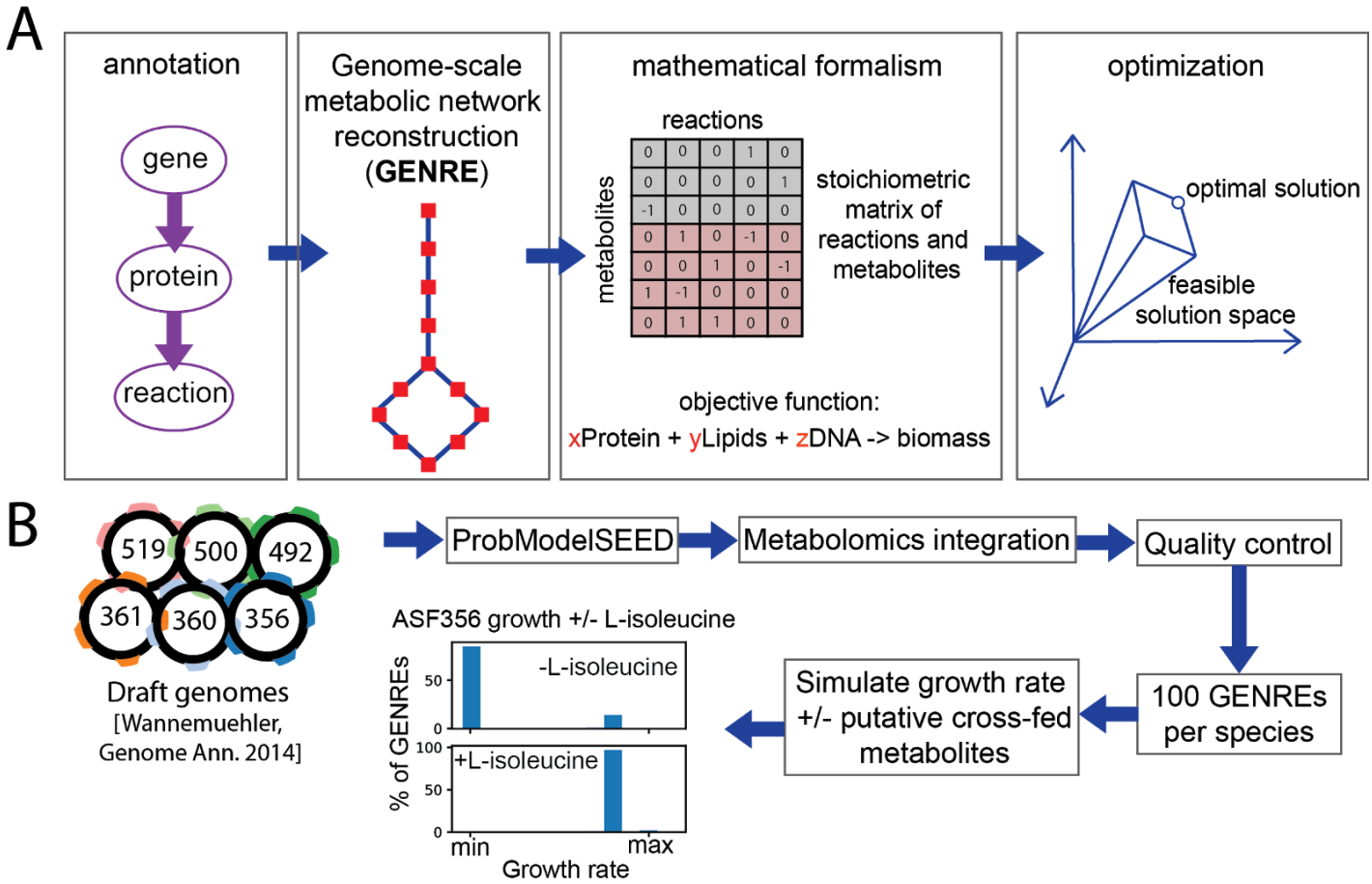

C

EnsembleFBA predictions for ASF356 growth w/ and w/out putative cross-fed metabolites

Metabolite	L-alanine	L-isoleucine	L-proline	L-valine	choline	formate
% GENREs metabolite is essential in	0	85	0	100	0	0
Mean biomass production with met.	0.079	0.079	0.079	0.079	0.079	0.079
Mean biomass production without met.	0.079	0.012	0.079	0.000	0.079	0.079

Figure S3. Computational model-driven interrogation of potential metabolic interactions and experimental validation of a cross-feeding interaction (related to STAR Methods, Draft genome-scale metabolic network reconstruction and analysis). **A)** Process for generating and applying a genome-scale metabolic network reconstruction (GENRE). **B)** Novel pipeline for constructing and analyzing ensembles of GENREs for the ASF strains. Details for each step in Materials and Methods. **C)** EnsembleFBA predictions of the influence of potentially cross-fed metabolites on growth of *Clostridium* ASF356. Biomass production values are for flux through the biomass reaction in units of $hour^{-1}$, and a metabolite was considered essential if removal led to flux through the biomass reaction of less than < 1E-5/hour. Predicted flux through biomass in the experimental medium without any supplement or metabolite removal is 0.079/hour.

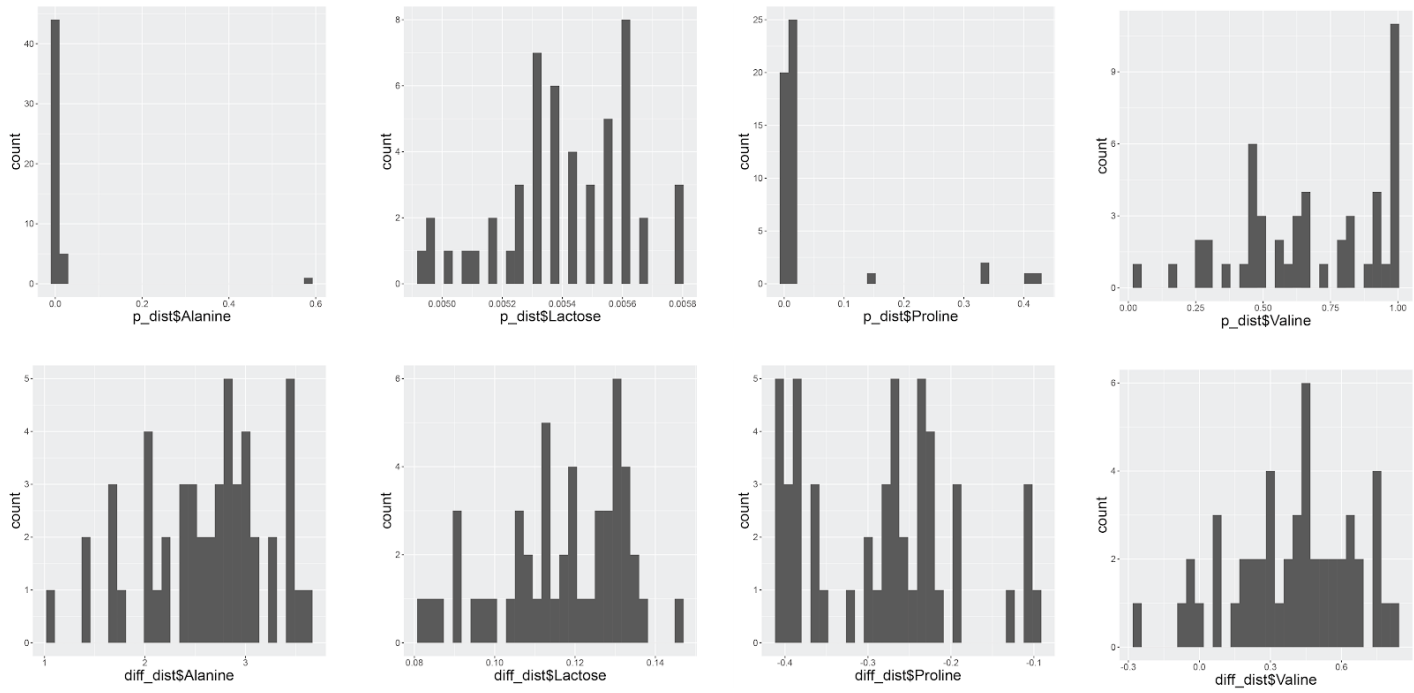

Figure S4. Selected examples of ConYE results using bootstrapped strain abundances (related to STAR Methods, Constant Yield Expectation (ConYE) model). Top row shows the distribution of ConYE *p*-values for each metabolite and bottom row shows the distribution of difference from the expected value for the same metabolite within each column. Examples are from the co-culture of *Clostridium* ASF356 and *Parabacteroides* ASF519. Distributions were generated by recalculating the average abundance of each strain in monoculture using leave-two-out bootstrapped samples prior to calculating the monoculture yield for each metabolite. N=50 samples with replacement for each monoculture.

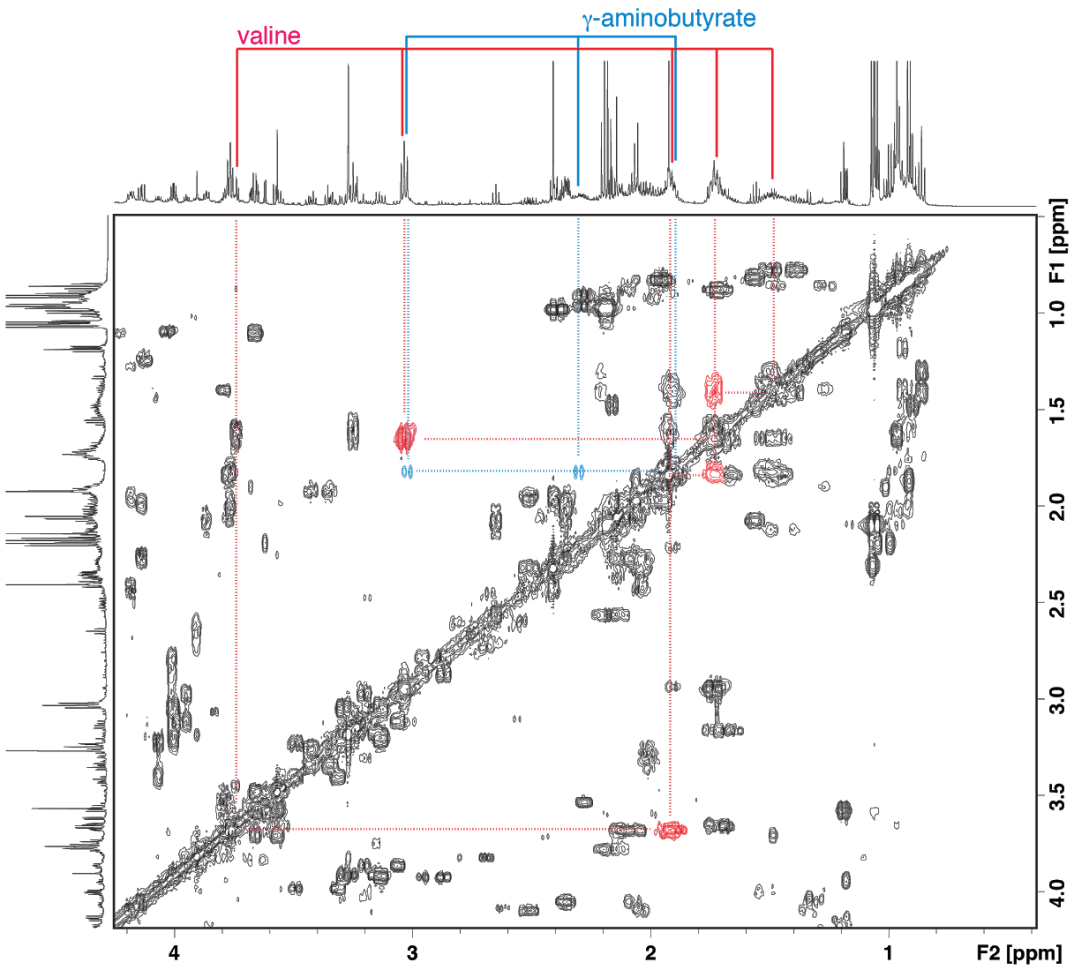

Figure S5. 2D ^{1}H NMR spectra collected on a single sample of supernatant from co-culture of *Clostridium* ASF356 and *Parabacteroides* ASF519 (related to STAR Methods, ^{1}H nuclear magnetic resonance spectroscopy-based metabolomics). 2D spectra show gamma-aminobutyrate, not 5-aminovalerate, in the region overlapping with valine in 1D. Peaks corresponding to valine shown in red, gamma-aminobutyrate shown in blue.

Table S1. Sequences for primers, probes, amplified products, and fluorophore and quencher pairs for each probe. Related to STAR Methods, Hydrolysis probe-based qPCR assay design.

strain	Fluor/quencher	gene	forward	reverse (reverse complement)	full_product	probe
ASF356	Cy5/BHQ2	WP_004034147.1|ASF356	TGGTGCTGCAACAGAAACAG	GGTATTGTTGCTGGTGGTGG	TGGTGCTGCAACAGAAACAGAAATGAAAGAGAAGAAATTAAGAATGGAAGATGCTTTAGCAGCTACAAGAGCAGCAGTAGAAGAAGGTATTGTTGCTGGTGGTGG	TGCTTTAGCAGCTACAAGAGCAGCAGTAGA
ASF361	FAM/BHQ1	WP_004049972.1|ASF361	GTCGGATCTTAGGCCACGAG	CAGTTGATGGGGGCATGAGT	GTCGGATCTTAGGCCACGAGGGGATCGGGATCGTCACTGAAGTTGCTAATGATGTAACTTCGCTCAAAGTCGGTGATCGCGTAAGTATTGCTTGGTTCTTCAAGGGGTGTGGATACTGTGAATACTGTACCACAGGTCGTGAAACTCTTTGTCGTAATGTACAAAATGCAGGTTACTCAGTTGATGGGGGCATGAGT	ATCGGGATCGTCACTGAAGTTGCTAATGAT
ASF492	FAM/BHQ1	WP_004053549.1|ASF492	CAGTGGAAGCTCTGCAGGAA	GGGGATGAAGAAGTCGGCAA	CAGTGGAAGCTCTGCAGGAAATGAGCCAGAAAGTAGACGGAAAAAATCACATTGCAAAAGTTGCGGCTATTTCCGCAGGGGATGAAGAAGTCGGCAA	TCACATTGCAAAAGTTGCGGCTATTTCCGC
ASF500	HEX/BHQ1	WP_023345698.1|ASF500	GGAACTATCTCCGGGGGACT	TTGCGTGCTGTTGTCAATGG	GGAACTATCTCCGGGGGACTGGGCGGCGTATCTGCCGCTGGAGCGGGAAATCCCTAAAAATGTCCGCAGAGCTATCGCTATGGAGTGGTCACAGCTTCGAGAGGAAAATTCACCCTTGCGTGCTGTTGTCAATGG	TGCCGCTGGAGCGGGAAATCCCT
ASF502	TR/BHQ2	WP_004070354.1|ASF502	GCGAAGTCCGTCAAGGTACA	CCGACAGAGTGGCTCAGATC	GCGAAGTCCGTCAAGGTACAGAAGGAAAATACCGTAATCGTAGACGGCTCCGGCGACAAGCAGGCGATTGCCGACAGAGTGGCTCAGATC	AATCGTAGACGGCTCCGGCGACAAGCA
ASF519	HEX/BHQ1	WP_010802098.1|ASF519	CGCAGCTTCTATCGCTGGTA	CTCCGATGAACCCGGGTATG	CGCAGCTTCTATCGCTGGTATGTTCCTGACAACAGAATGTGTAATCGCAGAGAAGAAAGAAGATACTCCTGCTATGCCTCCGATGAACCCGGGTATG	TGTTCCTGACAACAGAATGTGTAATCGCAG
ASF360	TR/BHQ2	WP_004039698.1|ASF360	AGCCGCTTTTTGGATTTGGG	TGGTGGATCGGCGTAATTCC	AGCCGCTTTTTGGATTTGGGCTACAATTGCGCAAATTGGTCATACAGTCCGTCGTTTGCATGATGCCAACTTTATCGGTTGGTGGTGGTGGATCGGCGTAATTCC	AGTCCGTCGTTTGCATGATGCCAACTTTAT

Table S3. Metabolites for which niche expansion was observed (related to Figure 6).

strains	metabolite
356,492	2-Oxoisocaproate
356,500	2-Oxoisocaproate
492,500	2-Oxoisocaproate
356,492	unknown26
356,500	unknown26
492,500	unknown26
360,361	Serine
361,500	unknown5
492,500	unknown5
356,492	Pyroglutamate
356,500	Pyroglutamate
492,500	Pyroglutamate
356,361	unknown25
356,361	Tryptophan
356,500	Tryptophan
361,500	Tryptophan
492,500	unknown16
360,492	unknown8
360,500	unknown8
492,500	unknown8
360,361	Leucine
360,492	Leucine
361,492	Leucine
361,500	Leucine
492,500	Leucine
361,500	Cystine
492,519	Nicotinamide
492,500	unknown2
500,519	Glycine
356,492	Phenylalanine
356,500	Phenylalanine
360,361	Phenylalanine
361,492	Phenylalanine
361,500	Phenylalanine
492,500	Phenylalanine
360,492	unknown12
360,500	unknown12
492,500	unknown12
492,500	unknown9
356,492	Aspartate
356,500	Aspartate
361,492	Aspartate
361,500	Aspartate
492,500	Aspartate
492,500	unknown7
356,500	Tyrosine
360,361	Threonine

360,500	Threonine
361,500	Threonine
361,500	unknown33
361,492	unknown3
361,500	unknown3
492,519	unknown4
361,500	Choline
360,492	unknown10
360,361	Succinate
361,492	Succinate
361,500	Succinate
492,500	Proline
492,500	Trehalose
492,500	unknown13
361,500	unknown1
492,500	Isoleucine
356,492	Methionine
356,500	Methionine
361,492	Propionate
361,500	Propionate
492,500	Propionate
361,500	Alanine
360,361	Valine
361,492	Valine
361,500	Valine
361,492	unknown18
356,492	Glutamate
361,492	Glutamate
492,500	UMP
356,492	Lysine
356,500	Lysine
360,361	Lysine
361,492	Lysine
361,500	Lysine
492,500	Lysine
492,500	Isocaproate
356,500	Asparagine
360,492	Asparagine
361,500	Asparagine
356,492	Isopropanol
356,500	Adenine
492,519	Cytosine
360,519	unknown32